NUMERICAL STUDY OF PASSIVE MIXING IN A 3-D HELICAL MICROMIXER HAVING BOTH INLETS AT OFFSET WITH WATER AND BLOOD AS FLUIDS

A PROJECT REPORT

SUBMITTED IN PARTIAL FULFILMENT OF THE REQUIREMENTS FOR THE AWARD OF THE DEGREE
OF

MASTER OF TECHNOLOGY
IN
THERMAL ENGINEERING

Submitted by:
AKASH SINHA
(2K20/THE/03)

Under the supervision of:
Dr. M. ZUNAID
(Asst. Professor)

DEPARTMENT OF MECHANICAL ENGINEERING
DELHI TECHNOLOGICAL UNIVERSITY
(Formerly Delhi College of Engineering)
Bawana Road, Delhi-110042

MAY, 2022

DEPARTMENT OF MECHANICAL ENGINEERING
DELHI TECHNOLOGICAL UNIVERSITY
(Formerly Delhi College of Engineering)
Bawana Road, Delhi-110042

CANDIDATE'S DECLARATION

I, **Akash Sinha** (Roll no: 2K20/THE/03) student of M.Tech. (Thermal Engineering) hereby declare that the project Dissertation titled "**Numerical Study of Passive Mixing in a 3-D Helical Micromixer Having Both Inlets at Offset with Water and Blood as Fluids**" which is submitted by me to the Department of Mechanical Engineering), Delhi Technological University, Delhi in partial fulfilment of the requirement for the award of the degree of Master of Technology (MTech.) is an original and not copied from any source without proper citation. This work has not previously formed the basis of any other Degree, Diploma Associateship, Fellowship or other similar title or recognition.

The current thesis work has resulted in the publication of two research articles in conferences with details as follows:

(1.) Title of the Paper: **Numerical Study of Passive Mixing in a 3-Dimensional Helical Micromixer with Two Inlets at Offset**.

Authors: Akash Sinha[1], Mohammad Zunaid[2]

Name of the Conference: 1st International Conference on

Design and Materials (ICDM) - 2021

Status of the Paper: Accepted

Date of Initial Submission of Paper: 23/10/2021

Date of Paper Acceptance: 24/12/2021

Date of Paper Publication: NA

(2.) Title of the paper: **Numerical Study of 3-D Helical Passive Micromixer having Both Inlets at Offset with Blood as Fluid**.

Authors: Akash Sinha[1] and Mohammad Zunaid[2]

Name of the Journal: 13th International Conference on Material Processing and Characterization

Status of the Paper: Published

Date of Initial Submission of Paper: 28/03/2022

Date of Paper Acceptance: 11/04/2022

Date of Paper Publication: 27/04/2022

AKASH SINHA
(2K20/THE/03)

DEPARTMENT OF MECHANICAL ENGINEERING

DELHI TECHNOLOGICAL UNIVERSITY

(Formerly Delhi College of Engineering)

Bawana Road, Delhi-110042

CERTIFICATE

I hereby certify that the Project Dissertation titled **"Numerical Study of Passive Mixing in a 3-D Helical Micromixer Having Both Inlets at Offset with Water and Blood as Fluids"** which is submitted by Akash Sinha, 2K20/THE/03 (Department of Mechanical Engineering), Delhi Technological University, Delhi in partial fulfilment of the requirement for the award of Master of Technology, is a record of the project work carried out by the student under my supervision. To the best of my knowledge this work has not been submitted for the award of any Degree or Diploma to this or any other Institute/University.

Place: Delhi

Date: 27.05.2022

Dr. M. Zunaid

Assistant Professor,

Department of Mechanical Engineering,

Delhi Technological University

(Formerly Delhi College of Engineering)

Bawana Road, Delhi-110042

SUPERVISOR

DEPARTMENT OF MECHANICAL ENGINEERING
DELHI TECHNOLOGICAL UNIVERSITY
(Formerly Delhi College of Engineering)
Bawana Road, Delhi-110042

ACKNOWLEDGEMENT

I would like to take this opportunity to extend my deepest gratitude towards my supervisor **Dr. M. Zunaid**, Asst. Professor, Department of Mechanical Engineering for supporting this research and also for his consistent guidance, motivation throughout this journey. I consider myself to be fortunate to be a part of his team and work under his mentorship.

I would also like to thank my teachers and colleagues at Delhi Technological University for assisting me in the pursuit of this project.

Finally, I am greatly thankful to my family and friends for their non-stop support and motivation. This work would have not been possible without them.

Akash Sinha
(2K20/THE/03)

ABSTRACT

The mixing of Newtonian fluid water and non-Newtonian fluid blood are numerically investigated in two different micromixers. The present study tackles the problem of time-consumption in mixing at the micro-level by introducing a micromixer named 3D helical micromixer having two inlets at offset (TDHM-TO). It is concluded that this micromixer requires comparatively less mixing channel length and provide much better efficiency than a Simple T-micromixer (STM). A detailed work has been done to examine the mixing process and performance, various streamlines, effective Reynolds numbers/mass flow rate for both the micromixers, and pressure drop by solving Navier-Stokes, species transport, and continuity equations for Reynolds numbers (8-400).

In the case of water as working fluid, for all ranges of Reynolds numbers, helical micromixer performed better than STM. TDHM-TO provides maximum efficiency of 97.32% at Re= 310 and minimum efficiency of 79.95% at Re= 8. STM shows comparatively poorer results with a mixing efficiency of just 43.23% at Re= 410.

The study with blood considers a wide range of mass flow rates (0.0004 kg/hr. – 0.10 kg/hr.). It is being found that, for all values of mass flow rate, TDHM-TO performed much better than STM. E.g., for flow rate= 0.07 kg/hr., TDHM-TO provide a mixing efficiency of 74.41% compared to 4.93 of STM which is about 65.2% more than that of STM. STM showed a very poor result compared to TDHM-TO with only 7.64% of maximum mixing efficiency obtained with the flow rate= 0.1 kg/hr. compared to 72.84% of TDHM-TO. This TDHM-TO micromixer can be, thus, utilized in many chemicals, biochemical, and biomedical industries because of its higher efficiency and lower mixing length.

TABLE OF CONTENTS

LIST OF FIGURES

LIST OF TABLES

NOMENCLATURE

L_a	The axial length of Simple T-mixer, µm
P_h	Pitch of the helical channel, µm
d_m	Mean diameter of the helical curve in TDHM-TO, µm
L_m	Mixing or peripheral length of TDHM-TO, µm
W_i	Width of the inlet channels, µm
W_0	Width of the outlet channel, µm
H	Height of the channel, µm
N	Number of turns in TDHM-TO
L_e	Exit length, µm
ρ	Density of the fluid, Kg/m^3
x, y, z	Cartesian co-ordinates
u, v, z	Velocity components of the flow field in x, y, z directions, m/s
$\vec{V}$	Velocity vector, m/s
t	Time, seconds
b_i	Body force component, N
τ_{ij}	Stress Tensor, N/m^2
λ	Volumetric dilation coefficient
δ_{ij}	Kronecker delta
P	Pressure, KPa
D_{AB}	Coefficient of molecular diffusivity
C_A	Concentration of species

n	Power-law index
K	Consistency index
H	Apparent Viscosity of Non-Newtonian fluid, Pa-s
$\dot{\gamma}$	Rate of shear
η_0	Zero shear rate viscosity, Pa-s
η_∞	Infinite shear rate viscosity, Pa-s
λ	Characteristic relaxation time
D	Rate of deformation Tensor
Re	Reynolds Number
V_m	Mean Velocity of the flow, m/s
D_h	Hydraulic diameter of the microchannel, µm
Mi	Mixing index, %
σ^2	Actual variance in the mass fraction of the fluid component
σ^2_{max}	Maximum variance
c_i	Mass fraction at sampling point i
c_{avg}	Average mass fraction at a cross-section
ṁ	Mass flow rate of blood, Kg/hr

CHAPTER 1

INTRODUCTION

1.1 Introduction to Microfluidics

The study of fluid flow at the microscale, i.e., the length scale of the systems being of the order of micrometres is termed as microfluidics. The concept of miniaturization of various chemical, biochemical, and biological analyses carries enormous advantages. First, there is a significant amount of reduction in the requirement of the sample size. For example, downscaling the linear scale by a factor of 10^4 will reduce the volume requirements by the order of $10^{12}$and such a lower volume of fluid helps in fast analysis and diagnosis. Second, shrinking down the actual size of chemical/ biological laboratories to the size of the chip will not only bring down the cost associated with set-up and running the laboratory in remarkable amounts but also makes the laboratory compact and portable. A lab on chip (LOC) device is an excellent example of a microdevice which consists of one or several laboratory functions on a single chip. These chips will also provide us with increased selectivity and sensitivity. Due to these advantages, Lab on a chip (LOC) technology has driven several critical research trends over the past few decades, particularly for applications in chemical and biological fields.

Although in microelectronics the behaviour of electrons remains almost the same even at the micro and nano scales, however, the scenario for fluids at the microscale is different with respect to the behaviour at macroscales. The physics of fluid flow changes drastically with length scales and one of the important dimensionless parameters characterizing the flow is the Reynolds number, Re. At micro-scales, the flow of fluid is highly influenced by the viscous forces of the fluid contrary to the macro-scales where the inertial forces play a major role in flow dynamics. If we have to imagine swimming at a microscale, our motion will stop instantly due to the opposing viscous forces whereas in macroscales we observe the motion to continue for a longer period and distance due to the presence of inertia. Some applications of the microfluidics are discussed below:

1.1.1 Application- Biomedical Diagnostics

One of the prominent applications of microfluidics is medical diagnosis. Currently, various microfluidic devices are being used for HIV diagnosis, pregnancy tests, screening of drug abuse, glucose biosensors, etc. This domain of microfluidics is termed as point-of-care (POC) which requires more exploration to produce several other devices that incur a low cost, are easy to use, and are portable making it feasible for a larger portion of population even living in the rural areas.

1.1.2 Application- Analysis of biological macromolecules

To understand the properties and behavior of biological macromolecules like the DNA, RNA, proteins, etc, proper stranding and sequencing are needed. One such example is the DNA hybridization through microfluidics. It involves breaking the double-stranded DNA structure into a single-stranded DNA sequence for further analysis of a disease or infection. Figure 1.1 illustrates the basic building block of DNA structure known as nucleotide comprising of Nitrogenous base, sugar, and negatively charged phosphate group.

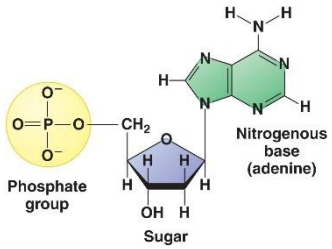

Figure 1.1 DNA nucleotide structure

1.1.3 Application- Drug delivery and blood extraction

The conventional methods of drug delivery and blood extraction involve using sharp syringes which are painful. Another drawback of using needles for drug delivery is the large time associated with the drug to be transported to the affected organ or area. However, employing microneedles is painless and can be directly used to deliver the drug close to the affected area reducing a significant amount of time due to the reduction in “drug path”. Several microdevices are also available for testing blood sugar

levels which are very helpful for diabetic patients who need to keep track of their sugar levels on a daily basis.

1.1.4 Application- Electronic cooling and Thermal management

With the reduction in the size of electronic components like microprocessors, Integrated circuits, etc. there comes a basic requirement of the effective dissipation of heat from these components to operate under the safe limit. Although the size of electronic components is getting smaller, however, the power input required to operate remains the same, and thus, removing the excess thermal energy from confined micro spaces is a challenge. Several droplets based microfluidic cooling systems and micro heat pipes have come out to be effective solutions to these problems. This domain is an extensive area of ongoing research and constant efforts are been made to construct optimal thermal designs in order to allow effective passive cooling for power components and modules.

1.1.5 Application- Mixing and Reactive system analysis

Several chemical and biomedical applications like micro-chemical reactors, polymerization, organic synthesis demand rapid mixing of fluids to obtain homogenized samples and fast reactions between the fluids. The current thesis involves an investigation of passive micromixers and a detailed Section 1.2 covers the field of these micromixers discussing various types, working, and applications.

1.2 Micromixers- An Overview

Micromixers are an essential part of various lab-on-chip (LOC) and micro total analysis systems (μTAS). In various microfluidic applications, the mixing efficiency of micromixers may affect the overall performance of the entire micro total analysis systems (μTAS). For example, fast mixing of cells, reagents, and organic solutions are essential in many bioengineering, biochemical systems, and nanomaterial synthesis. Efficient mixing not only improves the detection sensitivity but also brings down the analysis time by a notable factor. The physical phenomenon of mixing changes at microscales when compared to the mixing at macroscales. At macroscales, the mixing majorly depends on the convection mass transport which increases with the turbulent

nature of fluid flow due to the rise in momentum transfer, however, the flow at microscale is highly streamlined and laminar with no disordered random motion of the fluid. Hence, the mixing phenomenon is governed by molecular diffusion mass transport due to the dominance of viscous forces which demands the mixing fluids to stay in contact for a longer period of time and also requires long lengths of mixing channels. Since keeping the prolonged lengths of mixing channels rule out the basic idea and concept behind miniaturization of analysis systems, it is crucial to develop micromixers which are capable of giving effective mixing within a short period and lengths. Micromixers have numerous applications spread over a wide range of domains including:

- Polymerization
- Applications in crystallization
- Nuclear magnetic resonance (NMR) spectroscopy
- Organic synthesis
- The extraction process for chemical reactions
- Enzyme assay applications
- Biological Screening including both targeted cell sorting and selective sorting of biomolecules.
- Bio-analytical processes: cell separation, lysis, and DNA
- Protein folding

Based on the mechanism employed for mixing the fluids, micromixers can be broadly classified into categories namely, Active and passive micromixers.

1.2.1 Active micromixers

Active micromixers utilize external sources of energy like electrical field, magnetic field, vibrational energy, acoustic, rotational energy, pressure, etc as a stimulus to the mixing process in the microchannels [1]. These micromixers are complicated and require additional components which make it difficult to integrate into the micro-total analysis systems (μTAS). However, they give better control over the flow and the amount of mixing.

Electrical field-driven micromixers utilize the motion of electrically charged fluids in an electrical field (AC or DC) to disturb the interface of the mixing fluids which enhance the diffusion mass transport. This phenomenon is termed as the electro-hydrodynamic (EHD) instability [2]. Pressure field-driven micromixers are very common micromixers because of their simple construction and design. The basic design involves a simple T-channel with two micropumps to alternately inject the fluid into the mixing channel

making it a pulsatile flow. Employing this type of arrangement greatly enhances the interfacial area resulting in improved mixing efficiency [3]. Some work has also been reported with bubbles in a pressure field-driven micromixer. These bubbles when generated at a particular frequency will disturb the interface of the mixing fluids producing better mixing performance [4]. Micromixers driven by magnetic fields have magneto-fluids which are subjected to Lorentz forces with the help of magnets and electric fields. The magnetic field can serve both as a mixer and pump to drive the flow through the microchannel [5]. The electrodes are placed along the length of the conduit and the magnitude and direction of the magnetic field can be varied to control the flow dynamics of the electrolyte solution. Some designs also incorporate rotating magnets inside the channels to increase stirring action which will enhance the mixing efficiency [6]. A group of acoustically driven micromixers is based on bubble formation within the mixing channel to enhance the convective mixing. Some micromixers take advantage of the surface roughness of the walls of polydimethylsiloxane (PDMS) to form single or multiple bubbles. Another category of sound driven micromixer is which uses surface acoustic waves (SAW). The acoustic wave is made to pass the solid surface of the micromixer. The sound streaming increases the stirring effect which enhances the mixing index. Figure 1.2 illustrates and summarizes the classification of active micromixers.

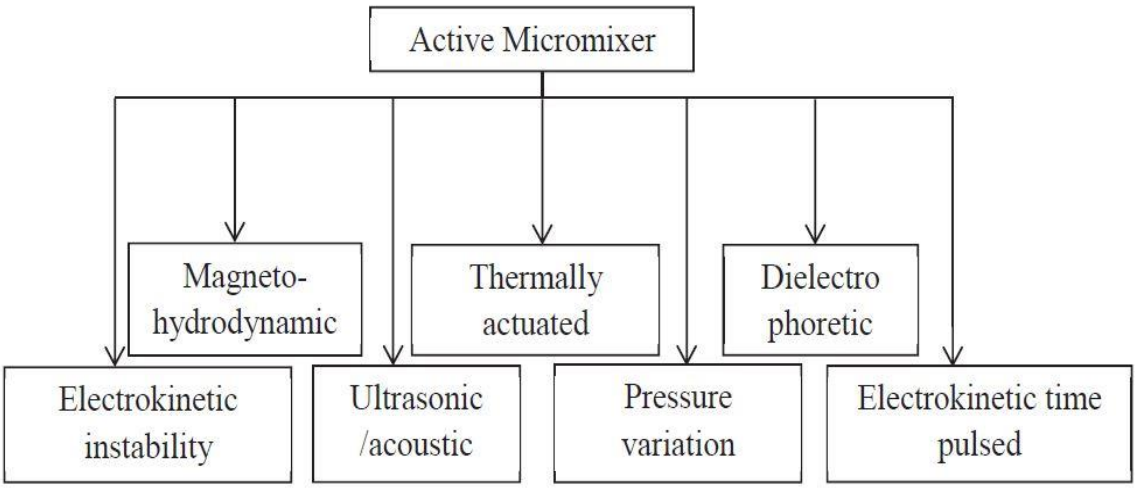

Figure 1.2 Types of Active Micromixer

Additionally, some micromixers also use the centrifugal forces imparted due to rotation to achieve good mixing. For example, Lab on CD micro-total analysis system has various components mounted on a disc which is rotated about an axis to evenly mix the fluids. The Coriolis effect comes into the picture due to the rotation and thus the mixing is strongly dependent on this component of force. The rotation per minute (rpm) of the disc can be varied to control the amount of mixing needed according to the requirements [7].

1.2.2 Passive micromixers

As mentioned above, active micromixers utilize external energy sources to enhance the mass diffusion process. However, passive micromixer also known as the static micromixer is different in the sense that it uses modification in geometry, shape, and size of the mixing channel to form vortices, produce chaotic advection, etc. The basic concept behind passive micromixer is to stretch and fold the flowing fluid number of times which magnifies the interfacial area of the mixing fluids increasing diffusion mass transport within a short distance and time. The major advantage of a passive micromixer is that it is simple to construct and integrate into a system and thus, the cost of running and manufacturing is very less making it an attractive mixer for exploration and several types of micromixers are developed by various scientists and researchers. Figure 1.3 depicts the types of passive micromixers. Since the current work of the thesis is based on passive micromixers, detailed background information and literature review are provided in chapter 2.

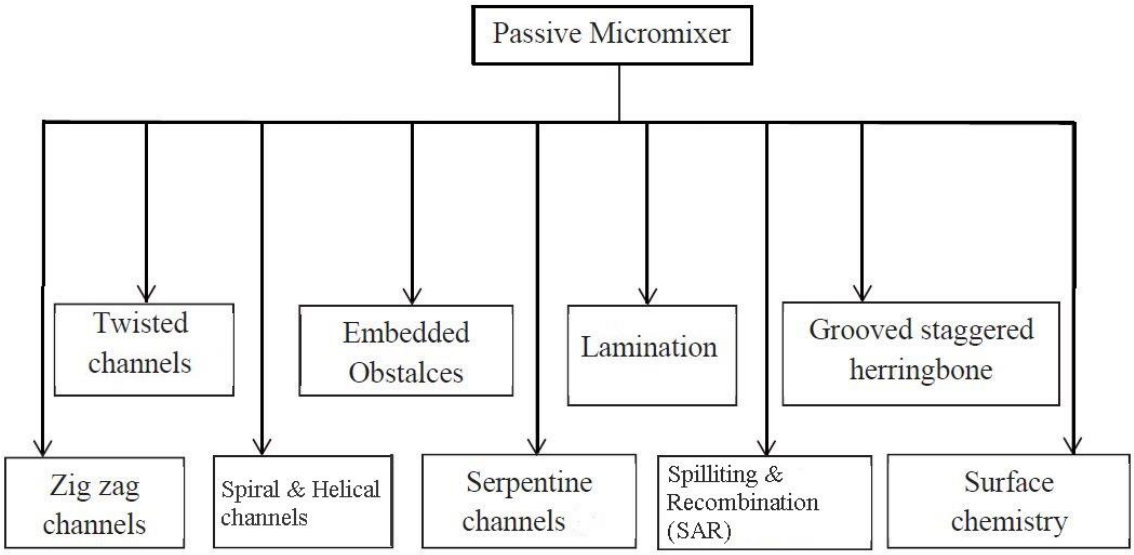

Figure 1.3 Classification of passive micromixers

1.3 Objectives of the Thesis

The thesis work investigates the mixing performance of both Newtonian fluid & non-Newtonian fluid blood in various effective passive micromixers and presents a deep study of the flow behavior of the fluids inside the microchannels. Computer-aided design (CAD) modelling is executed using the available commercial software SolidWorks whereas the numerical simulations were performed to solve the continuity, Navier-Stokes equation, and species transport equation of mass transport using the CFD solver in the software Ansys Fluent. The specific objectives of the thesis can be summarised as:

i. To evaluate the mixing efficiency of the 3-Dimensional Helical Micromixer with Two Inlets at Offset (TDHM-TO) and the conventional T-micromixer (STM) for a wide range of flow rates and Reynolds number, Re.

ii. Investigate the rheological flow characteristics of blood in microchannels and how does it differ from the flow behaviour of Newtonian fluid (Water in current work).

iii. To study the pressure drop between the inlet & the outlet of the micromixers to examine the energy requirements.

1.4 Thesis Outline

The current thesis consists of 5 chapters in total. The first chapter forms the basis of the work providing an introduction to the domain of microfluidics and micromixers. The second chapter consists of an in-depth discussion on the type of micromixers and the existing literature involving both experimental and numerical work. Chapter 3 discusses the governing partial differential equations used for the numerical solutions, a study on the grid sensitivity, behaviour of Newtonian and Non-Newtonian fluids, Validations of the computational approach with the existing literature, and numerical solution methodology implied in the study. Chapter 5 consists of the numerical solution obtained for STM and TDHM-TO with both Newtonian (water) and non-Newtonian fluid (Blood) as the working fluid in the micromixers. Finally, chapter 5 provides a brief conclusion of the work and the scope of the future in the field.

CHAPTER 2

LITERATURE REVIEW

Mixing fluids at the micro-scale level is a difficult task to do. Micro-scaled devices range from 10 to 100 micrometres and have several applications in biochemical industries, biological industries and other domains. They have several advantages such as less use of reagents, time-efficient, low cost, easily portable etc. The flow is laminar in micromixers due to the low Reynolds number hence it is tough to get the required level of mixing. In some cases, it can even demand a longer span of the micromixer to do the required level of mixing. Molecular diffusion (transfer and movement of molecules through a fluid) mainly pilots the mixing inside the micromixer which is a time-consuming process. According to the mode of operations, micromixers can be divided into two types as active micromixers and passive micromixers. An active micromixer is a micromixer that requires require external energy sources, such as Magnetic force, Ultrasonic, Dielectric-phoretic (phenomenon in which when a non-uniform electric field is exerted on a dielectric particle then it experiences force), etc. to

disturb the flow [1-7]. These micromixers are difficult to fabricate and are expensive. Whereas, a passive micromixer is a micromixer that does not require any external energy input. These micromixers only require fluid pumps and the pressure drop to drive the flow which is achieved by making changes in geometrical shapes or by providing obstacles in the path of fluid flow [8,9].

2.1 Simple T-micromixer

T micromixers have the most basic design of a micromixer and several studies have been done on it describing several flow regimes [10-16]. Fonte et al [11] numerically studied T-micromixer with square bends for a broad range of Reynolds numbers ranging from 60 to 300 using both conventional and novel lamellae-based models. The results from both analyses were, then, analysed by comparing with the existing study. It was concluded that, although, both methods resulted in better mixing efficiency when compared with the existing study, but lamellae model was computationally more efficient. Luo et al [12] performed a numerical analysis on a T micromixer which they called “baffled T-micromixer”. The baffled surface was used to provide more interfacial area to the fluid surface which in turn increased the mixing efficiency. Both mixing efficiency and pressure drop were unitized to calculate mixing ability of the fluid. Kurnia et al [15] studied a T micromixer with a twisted tape insert (a twisted strip). Their study evaluated several parameters such as Reynolds numbers, twisted tape width, nature of the twisted tape and permeability of the porous tape. It was concluded that using twisting tape can increase the mixing efficiency by two times that of a T micromixer. Dundi et al [16] evaluated the effects of swirl velocities at the inlets of a T micromixer and compared the result with a T micromixer without having swirl components. The results indicated a noticeable increase in mixing efficiency for all values of Reynolds numbers.

The Interfacial area (area of contact between the fluids) between the fluids also plays a major role in increasing mixing efficiency which can be increased by introducing helical and curved channels and shapes. This type of geometrical shape introduces a swirl effect on the fluid flow resulting in an improved diffusion process. Chen et al [17] studied and investigated an E-shape micromixer. It was concluded that a greater mixing efficiency can be reached by chaotic advection and splitting-recombination due to the design of the mixing channel. Highest achieved mixing efficiency was 94% at Re= 80.

Chen et al [18] in their another study, numerically investigated the performance of serpentine microchannel. A total of 6 micromixers with three different geometries (square-wave, multi-wave and zigzag) were studied with blue and yellow inked fluids. It was concluded that zigzag and square-wave micromixers were more efficient than multi-wave micromixers. Maximum efficiency of 95% was seen when Reynolds number was increased beyond 100.

Placing obstacles in the path of fluid flow is also an efficient way to improve the mixing efficiency. It helps in creating chaotic advection inside the microchannel. Chaotic advection can be defined as the phenomenon where a fluid particle attains complex behaviour and flow traces develop into complex fractals. Since the fluids now have to travel a longer distance, hence, it gets more time to diffuse. Md. Readul Mahmud [19] numerically investigated a modified T micromixer which contained circular and hexagonal shape obstacles with water as the fluid to mix. The study was done on a wide values of Reynolds numbers. The result showed that modified T micromixer with obstacles had much better performance than modified T micromixer without obstacles. Wu et al. [20] numerically evaluated a T-micromixer with obstacles at inlets called vortex-inducing obstacles (VIOs). The effects of various geometrical parameters on the mixing were studied. It was concluded that for higher values of Reynolds number (Re>27), the mixing efficiency increases with the increase in Reynolds number. Overall mixing got improved for every considered Reynolds number when compared with the simple T-micromixer. Li et al [21] studied three different micromixers on a wide values of Reynolds numbers (0.01-100). All three micromixers had obstacles placed at different plans A, B, and C named MSMA, MSMB, and MSMC respectively. It was concluded that the mixing efficiency of MSMA and MSMC was much better with mixing efficiency going beyond 90% for all the Reynolds numbers. Similar studies can be found in the references [22,23].

The fabrication of micromixer devices is a challenging issue when common techniques are used. It requires the use of unconventional manufacturing methods. Mondal et al [24] elaborated a speedy process for the fabrication of micromixers with poly-di-methyl-siloxane (PDMS- silicon based organic polymer). Two types of micromixers were fabricated- one raccoon type and the other serpentine type micromixer. The complete fabrication process took two steps, one is mould preparation and then fabrication. Mould was produced using Co_2 assisted lase machining on poly-

methyl-meth-acrylate (PMMA), and then micromixers were fabricated by the soft lithography technique. Tachibana et al [25] fabricated a 3D micromixer using lost-wax casting, a manufacturing method of rapid prototyping. 3D printing of hard wax resin was used for the mould preparation of lost-wax casting. By heating and washing with water, this hard was resin can be removed from a polydimethylsiloxane block. Similar fabrication techniques can be found in the references [26,27]. The fabrication of micromixers creates several structural problems which need to be looked at as well. There are several techniques that can be used to analyse such structural problems in the micromixer such as EFGM and MLPG which are meshless methods and are used to solve 1D elastostatics problems. Manish et al. [28] analysed various meshless methods and concluded that EFGM and MLPG both can be used to replace FEM and are much better alternatives. Also, EFGM is found to be more accurate than MLPG.

2.2 Curved and Helical Micromixers

Curved and helical design of a micromixer is a good way to enhance mixing inside a micromixer. This is because of the large interfacial area that a helical and curved shape provides between fluid species. This curved shape is the reason for the introduction of perpendicular secondary force, a force which causes swirling in the main flow. Mashaei et al [29] numerically studied a modified curved micromixer. Variations of several parameters such mixing index, pressure drops etc with Reynolds number were studied. The study was done with both Eulerian and Lagrangian viewpoints. It was concluded that the curved configuration of the micromixer is responsible for the increase in mixing. This curved shape generated an unsymmetrical transverse flow. Afzal & Kim [30] proposed a novel micromixer with a sinusoidal shape. Two fluids, ethanol and water, were used as the working fluid. A chaotic mixing induced by dean vortices was observed and hence the mixing improved due to the presence of secondary flow. The mixing index for shorter wavelength was compared with that of longer wavelength and the former was found to have a high value of mixing index due to the above-mentioned reason. Wang et al. [31] proposed a novel serpentine micromixer having an elliptical curve. It was observed that the direction of the flow kept changing due to the curved shape of the micromixer and dean vortices got introduced. The induced dean vortices were curve-dependent and kept changing as elliptical curves were changed. It was shown that the strongest dean force induced in the ellipse having the largest eccentricity. Balasubramaniam et al. [32] studied a spiral micromixer. It was concluded

that the dean vortices induced due to the curved shape of the microchannel were responsible for the primary diffusion. The spiral channel with different cross-sections (semi-circular, trapezoidal) was experimentally investigated and it was concluded that both of them resulted in an improved mixing index with minimal change in the pressure drop. Refer to [33-36] for more studies on the helical micromixers.

2.3 Concluding Remarks from Literature Reviews

From the above-mentioned literature reviews, it can be concluded that, although, several studies have been done on various types of geometries but the helically shaped micromixers still need some work. Hence in the present study, a helical micromixer has been evaluated for its mixing efficiency for a broad range of mass flow rates of blood and Reynolds number for water. The results are then compared with the existing literature of T-micromixer. This helical micromixer has two inlets and the axis of these rectangular cross-section inlets are at offset. As mentioned earlier, blood and water have been taken as the working fluid. Both the mixing efficiency and pressure has been evaluated for the helical micromixer and has been compared with STM. Carreau-Yasuda model [30], [37] was used to capture the Non-Newtonian behaviour of viscosity of blood and for Newtonian fluid, water was considered.

CHAPTER 3

METHODOLOGY AND MODELING

The numerical methodology to investigate the passive mixing include the development of flow domain, mesh generation, employing CFD-solver to iteratively solve the discretized governing equations, and finally, CFD-post processing to visualize the flow and mass transport between the fluids. Chapter 3 discusses the necessary governing partial differential equations that are continuity, the Navier-stokes equation, and the species transport equation to capture the molecular diffusion during the mixing. Since the current study involve examining the behaviour of both Newtonian fluid water and non-Newtonian fluid blood, the appropriate model used to capture the rheological behaviour of blood is explained in detail and the relevant modifications in the governing partial differential equations due to the non-Newtonian behaviour of blood is considered. The crucial boundary conditions and schemes used in the CFD solver are also discussed in detail in section 3.4. Section 3.6 elaborates on the mesh generation phenomenon and grid sensitivity analysis, i.e., comparing the results concerning the size of the grid used in the flow domain. Finally, in section 3.7, the validation of the computational method employed in this thesis is presented. The results for both

Newtonian and Non-Newtonian were compared with the work accomplished in the existing literature.

3.1 Model and domain description

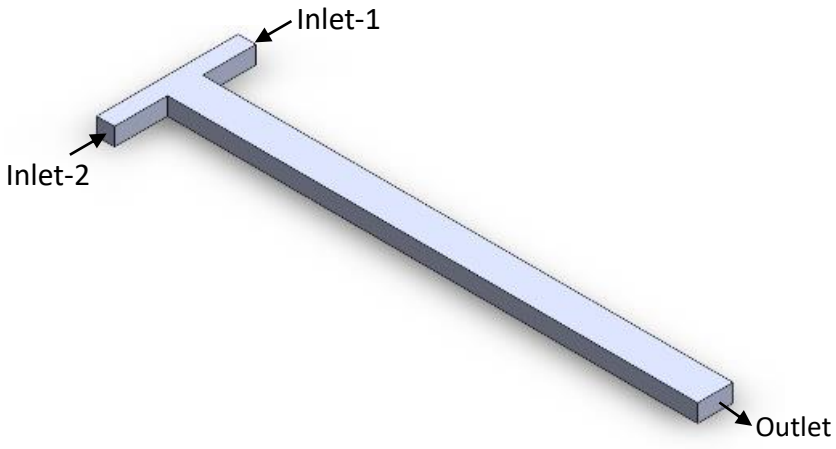

Figure 3.1 A Simple T-micromixer

Both the selected micromixers have been shown in the Figure 3.1 and 3.2. Both the micromixers, STM and TDHM-TO, have a rectangular cross-sectional area of dimensions 100×100μm at the inlet and 200*100μm at the outlet. The axial length of the STM is taken to be 3000μm (La). DHM-TO has two inlets that are at an offset to each other as can be seen from the figure 1(b). All geometrical parameters of TDHM-TO such as pitch (Ph), axial length (La) and Inlet and outlet width (Wi & W0) has been shown in the Figure 3.3. The diameter of the helix curve is 380mm. For the calculation of the velocity of fluid from the Reynolds number, the hydraulic diameter of the micromixer has been taken. All other dimensions of TDHM-TO are mentioned in Table 3.1. The mixing length or the peripheral length of the helical channel can be calculated by the following relation

$$L_m = N\left[\sqrt{(\pi d_m)^2 + P_h}\right] \tag{3.1}$$

Where N denotes the number of turns in the helical curve.

Table 3.1 Various dimensions of micromixer geometries

Geometric Parameter	**Values (μm)**

Width of the inlet of STM and TDHM-TO (Wi)	100
Width of the outlet of the channel (W0)	200
Hight of the channel (H)	100
Pitch of the curve (Ph)	370.57
The total axial length of the helical curve (La)	1411.71
Mean diameter of the curve (d)	380

To perform a comparative study, two different comparisons were studied. First, the mixing evaluation is done with STM and then with TDHM-TO.

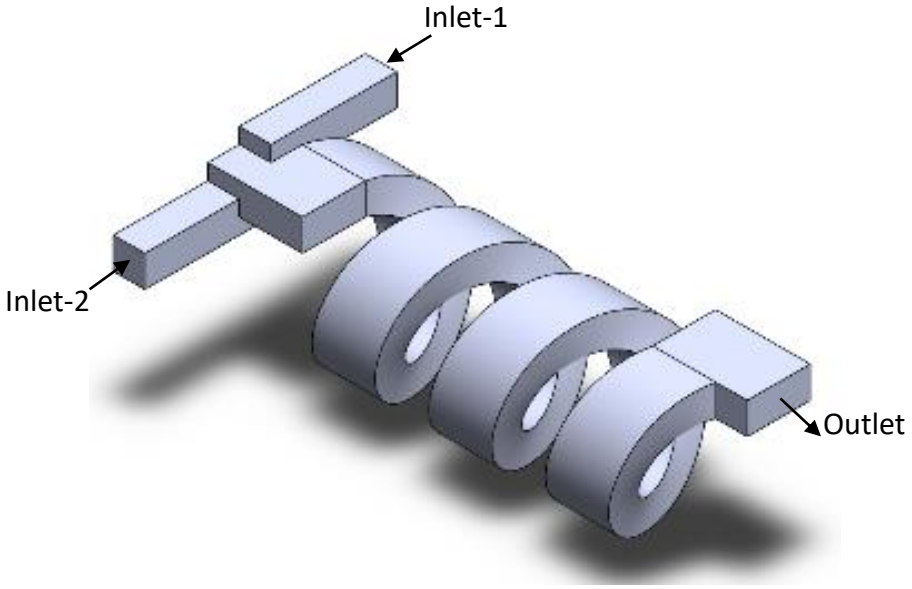

Figure 3.2 3-Dimensional Helical Micromixer with Two Inlets at Offset (TDHM-TO*)*

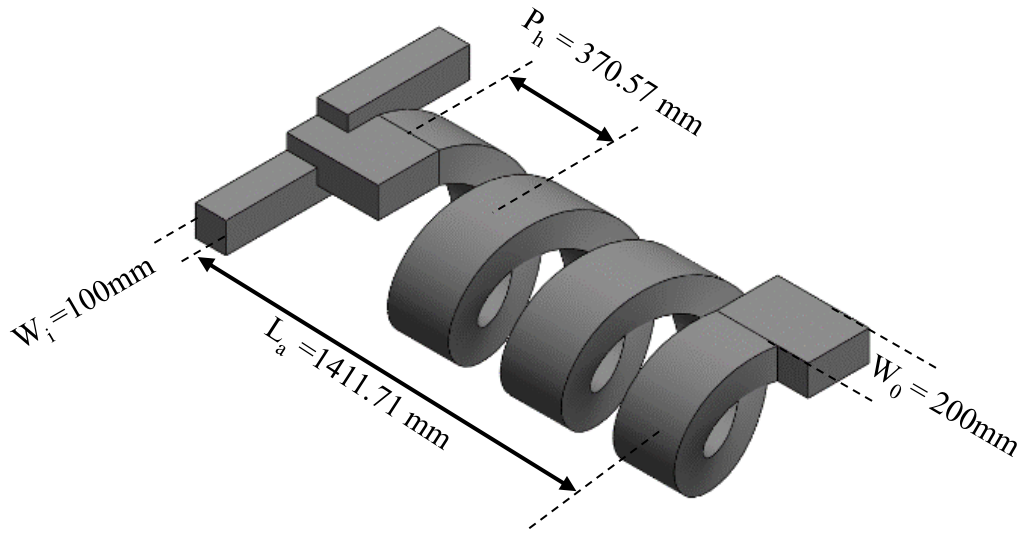

Figure 3.3 Parameters chosen to define the TDHM-TO

3.2 Governing equations

3.2.1 The continuity equation

The continuity equation represents the phenomenon of mass conservation. The general equation of continuity in differential form cartesian coordinates is given as

$$\frac{\partial(\rho)}{\partial t}+\frac{\partial(\rho u)}{\partial x}+\frac{\partial(\rho v)}{\partial y}+\frac{\partial(\rho w)}{\partial z}=0 \tag{3.1}$$

Where ρ is the density of the fluid. u, v, w represents the velocity components of the flow field in x, y, z directions respectively and t is the time. Although equation 3.1 represents the general form, the equation simplifies due to several assumptions including steady and incompressible flow in the case of Newtonian fluids.

$$\frac{\partial u}{\partial x}+\frac{\partial v}{\partial y}+\frac{\partial w}{\partial z}=0 \tag{3.2}$$

The equation can also be written in an alternative form using the del operator representing the divergence of the velocity vector is given by equation 3.3.

$$\nabla.\vec{V}=0 \tag{3.3}$$

Where, $\vec{V}$ is the velocity vector and ∇ is the del operator

$$\nabla = \frac{\partial}{\partial x}\hat{\imath} + \frac{\partial}{\partial y}\hat{\jmath} + \frac{\partial}{\partial z}\hat{k} \tag{3.4}$$

$$\vec{V} = u\hat{\imath} + v\hat{\jmath} + w\hat{k} \tag{3.5}$$

The dot product of del operator and velocity is known as the divergence of the velocity field.

3.2.2 Navier-stokes equations

The Navier-stokes equations are considered to be the fundamental equation of fluid dynamics as it is derived from the basic law of conservation of momentum. This equation consist of the body force terms that act on a differential fluid element when it is placed in a gravitational field, electrical field, magnetic field, etc or combination of these and the surface forces including both normal & shear stresses arising due to the pressure and viscid behavior of the fluid, respectively. The most generalised form of the momentum equation is as follows written with the index notation.

$$\frac{\partial(\rho u_i)}{\partial t} + \frac{\partial(u_i u_j)}{\partial x_j} = \frac{\partial(\tau_{ij})}{\partial x_j} + b_i \tag{3.6}$$

The right hand of the equation represents the sum of all the forces acting on the fluid element. Where, b_i is the body forces i.e., the force which is acting on every single particle of the fluid, τ_{ij} is the stress tensor given by:

$$\tau_{ij} = -p\delta_{ij} + \lambda\frac{\partial u_k}{\partial x_k}\delta_{ij} + \mu\left[\frac{\partial u_i}{\partial x_j} + \frac{\partial u_j}{\partial x_i}\right] \tag{3.7}$$

Where δ_{ij} is Kronecker delta, whose value is 1 when i=j and zero (0) for i≠j. λ is the volumetric dilation coefficient, μ is the coefficient of dynamic viscosity and $\frac{\partial u_k}{\partial x_k}$ signifies the volumetric deformation, whereas $\left[\frac{\partial u_i}{\partial x_j} + \frac{\partial u_j}{\partial x_i}\right]$ is the deformation caused due to shear stresses which act on the fluid element.

Since the fluid flow in the present work is assumed to be steady incompressible flow, the force due to the gravitational field is neglected and implying the stokes hypothesis, the equation 3.6 can be written for x, y and z-direction respectively as

$$\rho\left(u\frac{\partial u}{\partial x}+v\frac{\partial u}{\partial y}+w\frac{\partial u}{\partial z}\right)=-\frac{\partial p}{\partial x}+\frac{\partial \tau_{xx}}{\partial x}+\frac{\partial \tau_{yx}}{\partial y}+\frac{\partial \tau_{zx}}{\partial z} \tag{3.8}$$

$$\rho\left(u\frac{\partial v}{\partial x}+v\frac{\partial v}{\partial y}+w\frac{\partial v}{\partial z}\right)=-\frac{\partial p}{\partial y}+\frac{\partial \tau_{xy}}{\partial x}+\frac{\partial \tau_{yy}}{\partial y}+\frac{\partial \tau_{zy}}{\partial z} \tag{3.9}$$

$$\rho\left(u\frac{\partial w}{\partial x}+v\frac{\partial w}{\partial y}+w\frac{\partial w}{\partial z}\right)=-\frac{\partial p}{\partial z}+\frac{\partial \tau_{xz}}{\partial x}+\frac{\partial \tau_{yz}}{\partial y}+\frac{\partial \tau_{zz}}{\partial z} \tag{3.10}$$

The Navier-Stokes equation utilizes the divergence of the stress tensor, $\nabla.\tau$, The stress tensor can be represented in the form of a 3X3 matrix as

$$\tau=\begin{bmatrix}\tau_{xx} & \tau_{xy} & \tau_{xz}\\ \tau_{yx} & \tau_{yy} & \tau_{yz}\\ \tau_{zx} & \tau_{zy} & \tau_{zz}\end{bmatrix}=\begin{bmatrix}-p+2\mu\frac{\partial u}{\partial x} & \mu\left(\frac{\partial v}{\partial x}+\frac{\partial u}{\partial y}\right) & \mu\left(\frac{\partial w}{\partial x}+\frac{\partial u}{\partial z}\right)\\ \mu\left(\frac{\partial v}{\partial x}+\frac{\partial u}{\partial y}\right) & -p+2\mu\frac{\partial v}{\partial y} & \mu\left(\frac{\partial w}{\partial y}+\frac{\partial v}{\partial z}\right)\\ \mu\left(\frac{\partial w}{\partial x}+\frac{\partial u}{\partial z}\right) & \mu\left(\frac{\partial w}{\partial y}+\frac{\partial v}{\partial z}\right) & -p+2\mu\frac{\partial w}{\partial z}\end{bmatrix} \tag{3.11}$$

The viscosity, μ is a property of the fluid. It can be a constant as in the case Newtonian fluids, however, it may vary with the temperature, time, and the shear strain rate. These types of fluids fall under the category of non-Newtonian fluids. Section 3.3 briefly discusses both Newtonian and Non-Newtonian fluids and also introduces the Carreau-Yasuda model which is employed to numerically capture the rheological behaviour of the non-Newtonian Blood studied in the thesis.

3.2.3 The species transport equation

The flow at the microscale is purely laminar, therefore the only possible way by which mixing can occur between two fluids is through the diffusion of molecules from one fluid to the other once they come into the direct contact. To visualize and quantify the mixing phenomenon, the equation of conservation of species needs to be solved in the

flow domain with correct boundary conditions. The species transport equation of advection-diffusion type in the for a steady-state flow is given as follows.

$$\left(\vec{V}.\nabla\right)C_A = D_{AB}\left[\frac{\partial^2 C_A}{\partial x^2} + \frac{\partial^2 C_A}{\partial y^2} + \frac{\partial^2 C_A}{\partial z^2}\right] \tag{3.12}$$

Where, $\vec{V}$ is the velocity vector, C_A is the concentration of species A and D_{AB} is the coefficient of molecular diffusivity.

3.3 Newtonian and Non-Newtonian fluids

According to Newton's law of viscosity, at constant temperature and pressure, the simple shear stress (τ) is proportional to the shear rate ($\dot{\gamma}$) and the constant of proportionality is commonly known as the dynamic viscosity (μ). It infers that the shear stress increases linearly with an increase in the shear rate. The fluids which demonstrate this type of behaviour are called Newtonian fluids. Most of the fluids which possess low molecular weight such as various organic and inorganic liquids, molten metals, water, and a wide variety of salt solutions exhibit Newtonian behaviour when acted upon by the shear stress causing the fluid flow. It is observed that with an increase in either temperature or pressure, the viscosity of gases tends to increase due to the enhancement in the molecular collision as a result of the increased energy content of the gas, whereas in liquids the viscosity decreases with the increase in temperature due to the weakening of the force of attraction between the molecules present in the liquid. On the whole, the higher the viscosity of a substance, the more resistance it will exhibit to the flow and thus will require more power to pump the fluid and transport it from one location to the other. Contrary to the Newtonian fluids, non-Newtonian fluids do not display a linear relationship between the stress-strain rate and a deviation is observed as depicted in figure 3.4 which shows stress-strain curves for different non-Newtonian fluid. It means that the apparent viscosity of the fluid defined as $(\tau/\dot{\gamma})$ is not constant and is a function of either τ or $\dot{\gamma}$. Additionally, the viscosity of some fluids also depends on the time period, and hence non-Newtonian can be classified into two broad categories of time-dependent and time-independent fluids. Since our study is limited to modelling the hemodynamic of blood, which is a shear-thinning time-independent non-Newtonian fluid, the discussion is restricted to just the time-independent fluids and these fluids can

further be classified into shear-thickening, shear-thinning, and visco-plastic behaviour type.

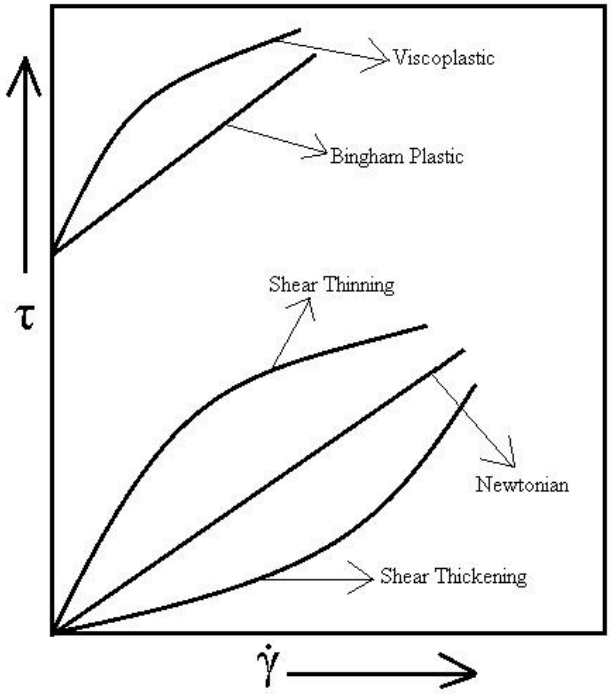

Figure 3.4 Qualitative curves for different types of fluids

The most common model employed to model the non-Newtonian characteristics is the power-law model or also known as the Ostwald de Waele Equation given as

$$\tau = K(\dot{\gamma})^n \tag{3.13}$$

Where K is the consistency index and n is the power-law index. The apparent viscosity, η is obtained by dividing the shear stress with the rate of shear.

$$\eta = \frac{\tau}{\dot{\gamma}} = K(\dot{\gamma})^{n-1} \tag{3.14}$$

It is well understood that for $0< n<1$, $\left(d\eta/d\dot{\gamma}\right)$ will always yield a negative value which implies that with the increase of the shear rate, there will be a reduction in the shear stress component of the fluid. The fluids presenting this type of behaviour are termed as shear-thinning fluids. Smaller the value of n, more shear-thinning is the fluid. Blood, various polymer solutions, and suspensions like bentonite-in-water are good examples of shear-thinning fluids. However, when the value of n is greater than 1, the behaviour tends to reverse, i.e. with an increase in shear strain, the value of shear stress also increases. This type of fluids falls under the category of shear-thickening behaviour

which can be readily witnessed in a corn starch and water mixture. For the case of n=1, the fluid showcase Newtonian rheology. The model employed to numerically understand the flow and mixing behaviour of blood in microchannels is the Carreau-Yasuda model as discussed briefly in the upcoming section

3.3.1 The Carreau-Yasuda model

Blood is a non-Newtonian fluid and to capture its viscosity change with change in strain rate, there are several models. One such model is the Carreau-Yasuda model. This model has been used by several analysts and researchers [37], [38], [39]. Following is the equation given by this model which expresses viscosity as a function of strain rate:

$$\eta(\dot{\gamma}) = \eta_0 + (\eta_0 - \eta_\infty)[1 + \lambda(\dot{\gamma})^a]^{(n-1)/a} \quad (3.15)$$

Where η_∞ denotes infinite shear rate viscosity, η_0 denotes zero-shear viscosity, n represents the characteristic relaxation time, and a is an empirical constant. The constant values of $\eta_0, \eta_\infty, \lambda, a \; and \; n$ are 0.1600 Pa s, 0.0035 Pa s, 8.2 s, 0.64 and 0.2128 respectively. The viscosity of blood is 1,058 kg/m^3 and the value of diffusivity is taken to be 2.8 × 10 $^{-10}$ m^2/s. The values have been taken from a previous work of Abraham et al [40].

Also, in the equation (3.15), $\dot{\gamma}$ is given by following equation,

$$\dot{\gamma} = \sqrt{2 \times (D : D)} \quad (3.16)$$

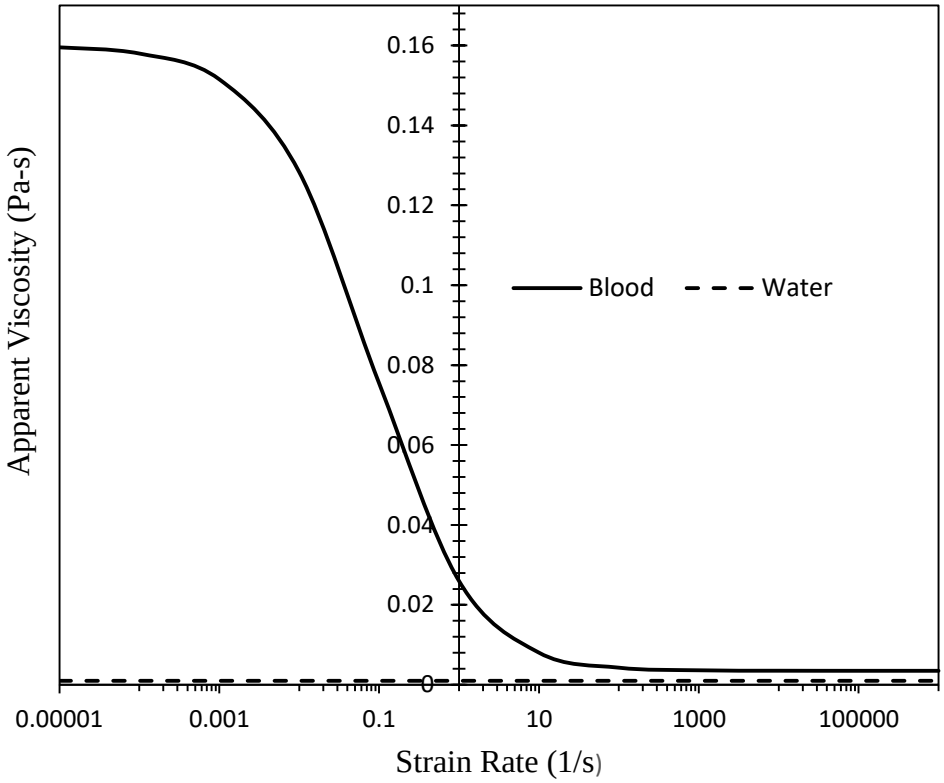

Figure 3.5 Apparent viscosity vs strain curve for blood and water

Here, D represents the tensor deformation rate. Figure 3.5 represents the change in apparent viscosity with the change in strain rate. The graph is continuous is nature and seems to have constant value of apparent viscosity when strain rate is either too low or too high hence behaves like a Newtonian fluid. At very low mass loading ($\dot{\gamma} \leq 0.001$), the blood is highly viscous (η_o = 0.1600 Pa-s) compared to the constant viscosity of water (0.001 Pa-s) whereas at higher values of strain rate or high mass loading the blood viscosity seems to have very small deviation from the viscosity of water. The graph becomes asymptotic at high strain rate but a difference of 0.0025 Pa-s in the viscosity can still be observed between water and blood at lower values of strain rate.

3.4 Numerical Solution method

The flow domain of the micromixers is generated using the readily available CAD modelling software SolidWorks. The modelled flow domain is then discretized into small elements and solved numerically using the CFD solver of ANSYS fluent which employs finite volume method. This section discusses the coupling and discretization

schemes, boundary conditions, and properties of the fluids used to solve the discretized equations.

3.4.1 Coupling and spatial discretization schemes

"Pressure-Based" solver and "steady" model have been used in the current analysis. Two models, "Laminar" and "Species Transport" models have been used in ANSYS fluent. For pressure-velocity coupling, "SIMPLEC" algorithm has been used and for spatial discretization of pressure, momentum and continuity, "second order upwind" has been selected. The residual for all the mentioned equations is set to 10^{-14} as the convergence criterion. Table 3.2 presents a summary of the numerical schemes employed in the computational simulations when blood is the working fluid.

Table 3.2 Solution methods used for CFD solutions

Pressure-velocity coupling	**SIMPLEC**
Pressure	Second-order
Gradient	Least squares cell-based
Momentum	Second-order upwind
Species	Second-order upwind

3.4.2 Boundary Conditions

There are two inlets in both the micromixers. For Newtonian fluid water, water is fed in inlet 1 with species concentration of "1" and water-dye is fed in inlet 2 with species concentration "2". Velocity of the fluids is being calculated using the following equation based on Reynolds number, Re.

$$Re = \frac{\rho V_m D_h}{\mu} \tag{3.17}$$

Where, V_m is the mean velocity of the flow, D_h is the hydraulic diameter of the microchannel, and ρ is the density of the fluid.

"Gauge pressure" at the outlet of the micromixers is considered to be "0". "Stationary wall" and "No-slip" conditions were selected in the "wall" section. Zero specific pressure is specified at the outlet of the mixer. For Non-Newtonian fluid blood, blood is

fed in inlets 1 and 2 with species concentrations of "1" and "0" respectively with velocities calculated using mass flow rate. Rest all the boundary conditions are the same as it was for the Newtonian fluid water.

3.5 Quantification of Mixing

The degree of mixing is obtained by calculating the parameter Mixing index (MI) in the microchannel at any particular location. MI is evaluated by following equation

$$Mi = \left(1 - \sqrt{\frac{\sigma^2}{\sigma_{max}^2}}\right) \times 100 \tag{3.18}$$

$$\sigma^2 = \frac{1}{n}\sum_{i=1}^{n}\left(c_i - c_{avg}\right)^2 \tag{3.19}$$

Where σ^2 is the sum of variance in the species concentration of fluid at a particular location, whereas σ_{max}^2 denotes maximum variance. 'c_i' is the mass fraction at sampling point 'i', and 'c_{avg}' is the average value of mass fraction at that particular location. The total number of points taken on the plane is 'n' which is equal to 500. If 'MI′ is '0', it means that no mixing is taking place whereas, if 'MI' is '1', it denoted that complete mixing is taking place. For mixing involving two equal streams of fluid, the value of σ_{max}^2 is calculated to be 0.25. A total of 500 (n) points were selected at any particular location to capture the average value of mixing index at that location. This is done to improve accuracy.

3.6 Grid generation and sensitivity analysis

Grid generation is a crucial step in a CFD study. The quality and size of the elements used to divide the flow domain have a huge impact on the numerical results and its accuracy. Coarse mesh takes less computational time but has poor numerical prediction capability whereas fine mesh is proven to give better accuracy with higher computational time. Thus, selecting an optimized grid element size is necessary keeping both the accuracy and the computational time in mind. A grid sensitivity analysis is performed to observe the variation of variables like velocity, pressure drop, and mixing

index with a change in the number of elements or the grid size. Both the geometries of micromixers have been Figure 3.6 shows the generated mesh with tetrahedral element.

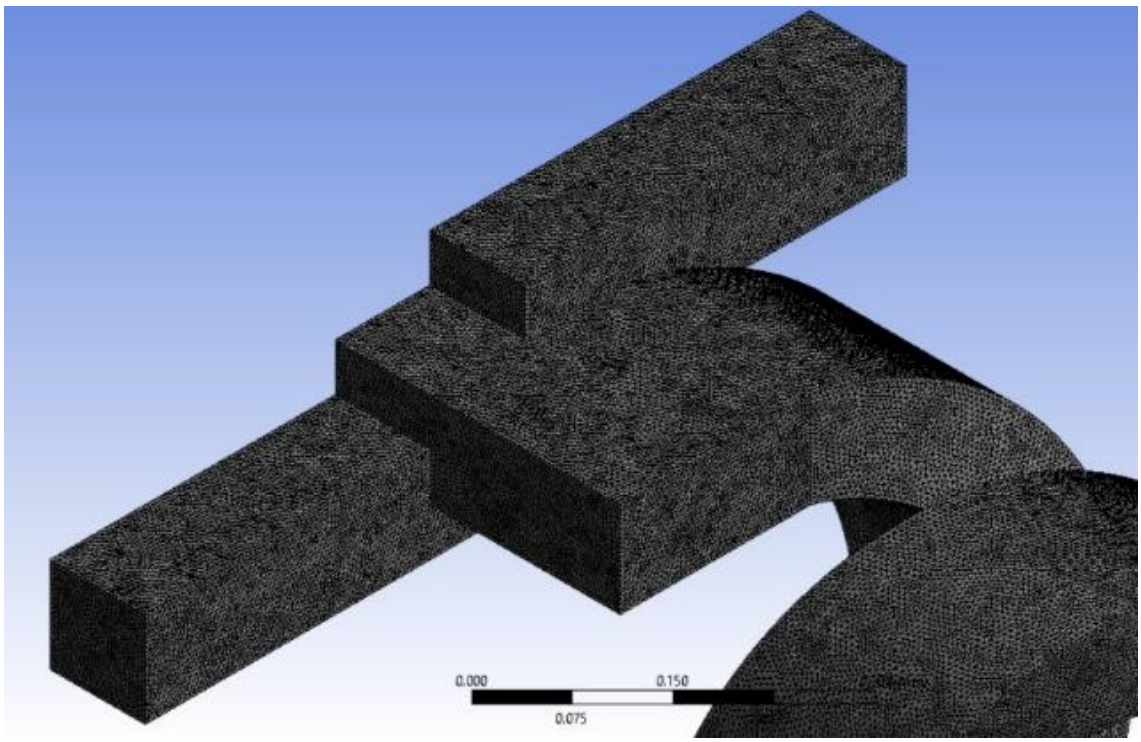

Figure 3.6 Mesh of TDHM-TO with 3.5 million tetrahedral elements

Tetrahedral elements are used whenever the fluid domain is complex as in the case of TDHM-TO. To start the simulation the optimum mesh element size and mesh element numbers are needed. To calculate the mentioned parameters, a grid independence test was done. For a mass flow rate 0.006 kg/hr., the simulation was performed and MI was noted for different mesh element sizes. It was observed that after three million mesh elements the change in the value of MI is very low (around 0.94%). Hence, this number of mesh elements was taken for the rest of the study. Figure 3.6 shows the graph between the number of mesh elements and the value of MI. Similarly, tests were carried out for the rest of the cases.

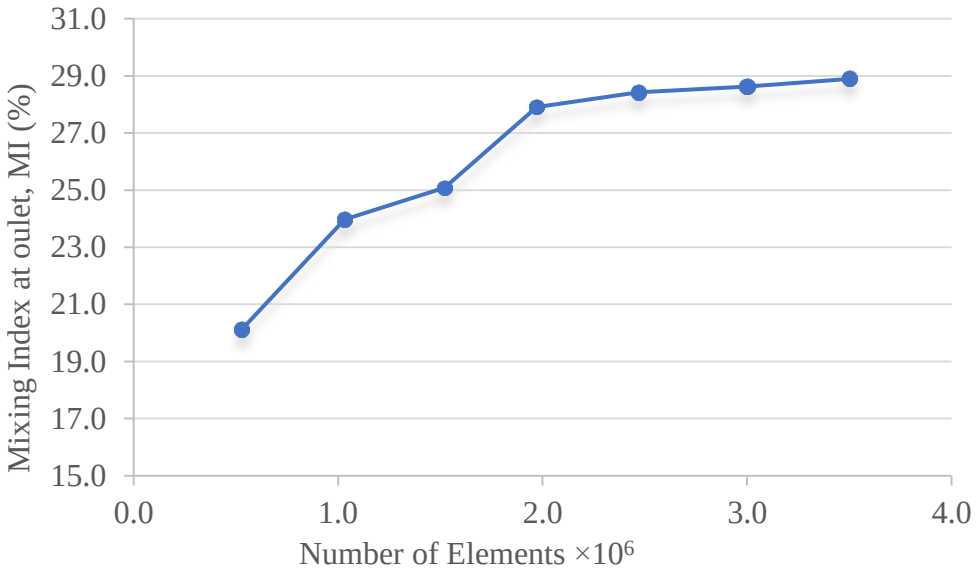

Figure 3.7 Grid sensitivity analysis

3.7 Validation of the computational approach

Numerical solutions are accompanied by various types of errors making the solutions doubtful on its accuracy and thus validation of the computational results obtained is must with the experimental data or with the existing published research data. Two different working fluids (Newtonian and Non-Newtonian) are used in the study and hence two different validation tests are performed to check the accuracy of the picked approach before proceeding with actual simulations.

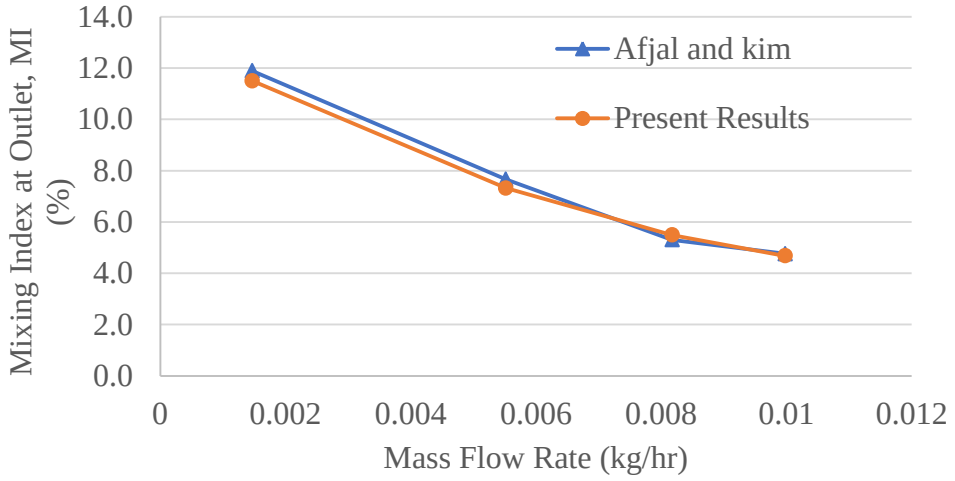

Figure 3.8 Mixing Index (blood): present study vs existing literature[30]

Afzal & Kim [30] performed numerical simulations to examine the performance of a serpentine channel micromixer and compared the results with the micromixer having a straight channel of length 4000 µm with a square cross-section of 100 µm × 100 µm. Working fluid is blood and the Carreau-Yasuda model was applied to study the rheology of blood at the micro-scale. Similar T-Micromixer is modelled and numerical simulations are performed under the same boundary conditions to ensure the reliability of the CFD approach. Figure 3.8 presents a comparison of mixing indexes obtained from the current study with that of the mixing indexes reported in the existing literature [30] at different mass flow rates of blood. The graph depicts that the current numerical results follow a similar trend and a good agreement of results is visible with a maximum deviation of 4.47 % at mass flow rate of 0.005 kg/hr.

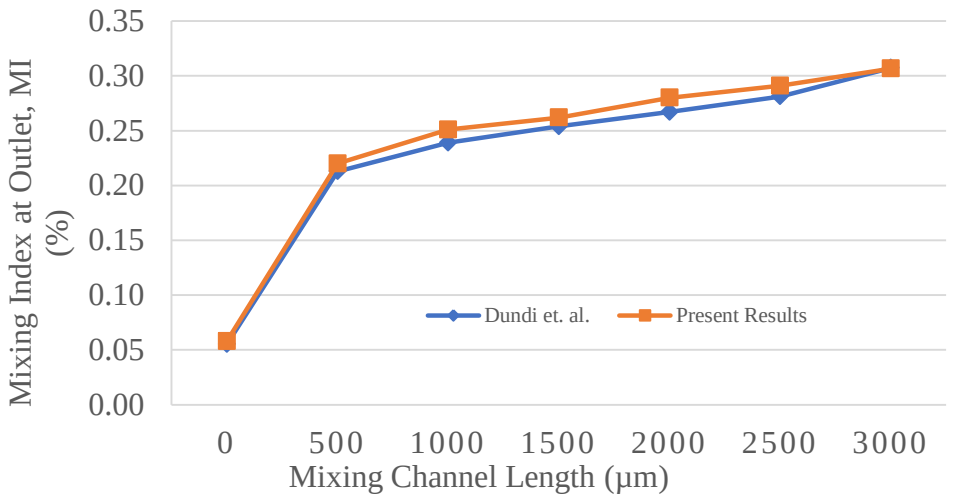

Figure 3.98 Mixing Index (water): present study vs existing literature[16]

Another validation test was performed to ensure the accuracy of the numerical results when the working fluid is changed to water. Dundi et al. [16] evaluated the flow characteristics and mixing performance of water (Newtonian fluid) in a simple T-micromixer of length 3000 µm and proposed to improve the mixing performance by providing swirl components of velocity at both the inlets. The results of the mixing index obtained from the numerical simulations conducted using similar dimensions and under the same boundary conditions are compared with the results presented by Dundi et al. [16] at Re=266. Figure 3.9 illustrates the variation of mixing at different length of the channels measured from the T-junction for Re=266 and also provide a comparison between the present obtained results and the mixing index calculated in the existing

literature. An average error of 3.39% is observed which is a satisfactory error. Furthermore, the contour representing the species concentration of water 1 (fluid 1) at the outlet plane is depicted in figure 3.10 and a similar trend is observed in the results of the mixing index proving the strength of the computational approach.

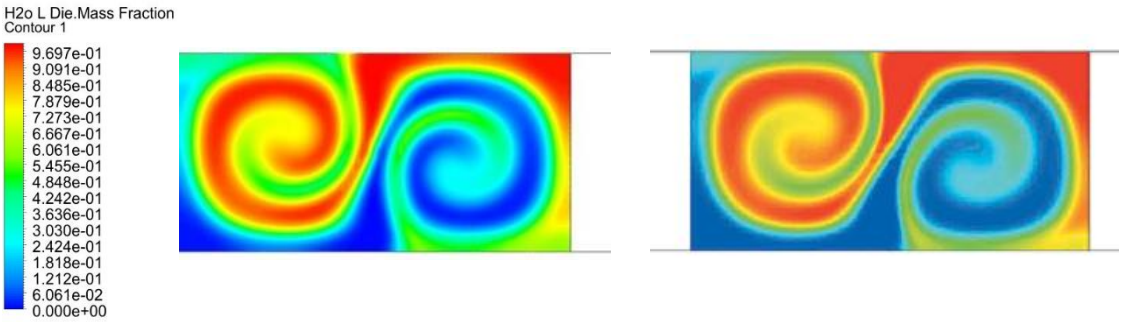

Figure 3.10 Contour based on species concentration at the outlet of (a) current study, (b) existing literature[16]

3.8 Summary

In this chapter, a brief explanation is presented of the mathematical modelling and governing equations used to examine the passive mixing performance of the micromixers. Also, the different approaches used for Newtonian fluid (water) and non-Newtonian fluid (Blood) are described in detail. The consideration related to the CAD modelling of the TDHM-TO and the meshing of the fluid domain is explained. Finally, the numerical solution techniques employed to obtain the mixing performance and the validation of this CFD approach is done using the data found in the existing literature.

CHAPTER 4

RESULTS AND DISCUSSIONS

The current chapter provides a thorough discussion of the numerical results obtained for both Newtonian fluid and non-Newtonian blood in STM and TDHM-TO. This chapter is divided into two major sections. The first section provides information on the mixing performance and flow characterization in a simple T-micromixer (STM) which has a straight channel for both water and blood as the working fluids. The second section includes numerical results of a 3-dimensional helical micromixer (TDHM-TO).

4.1 Mixing and flow analysis in Simple T-micromixer (STM)

As discussed in chapter 3, the total length of the straight mixing channel is 3000 μm with a cross-sectional area of 200 × 100 μm. It is important to note that the axial distance and the peripheral mixing length in a STM are equal whereas it differs for the case of TDHM-TO due to the introduction of 3-dimensional curvature. Flow and mixing behaviour of Newtonian and Non-Newtonian fluid (Carreau-Yasuda model) in a STM is discussed in section 4.1.1 and 4.1.2, respectively.

4.1.1 STM with Newtonian fluid (water) as the working fluid

Numerical simulation using Ansys Fluent is being performed to evaluate the mixing index and pressure drop of STM for an extensive range of Reynolds numbers (8-400). As described in several previously done studies, there are mainly three types of flow regimes formed in a T-micromixer with water as fluid– straight laminar flow regime, vortex flow regime and the engulfment flow regime. The present study found similar behaviour inside the STM with water as fluid. For low Reynolds number, i.e., for Re $\leq$75, the streamlines appeared to be parallel where both the species were flowing separately as can be

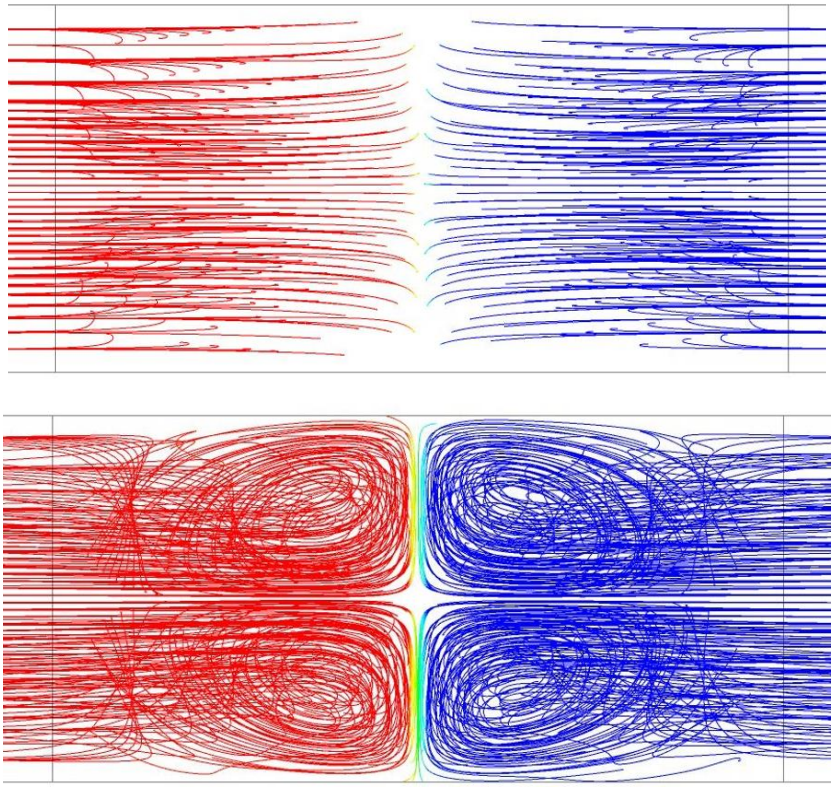

Figure 4.1 Species concentration-based streamlines in STM at (a) Re= 8 (b) Re= 125

visualized in Figure 4.1 (a) for Re= 8. Here, vortex flow doesn't occur and is hence called a straight laminar flow regime. In this regime, molecular diffusion is solely responsible for mass transfer between the fluid species. With the increase in Reynolds number, for Re=125, a small weak can be seen in Figure 4.1 (b). As can be seen from the Figure, the vortices are symmetrical about the vertical plane. This regime is called the vortex flow regime. But as can be seen from Figure 4.3, which shows the graph between mixing index and Reynolds number, the achieved mixing obtained from this range of Reynolds number doesn't show significant improvement. This is because, with the increase in Reynolds number, the residence time (the time spent by a fluid particle in the given volume) of fluid species decreases. STM showed this same behaviour till Re= 170, after that, the fluid created an engulfment flow regime. In this regime, the symmetry got broken up and strong mixing was observed due to chaotic advection and now the streams are no longer parallel. The mixing index has been calculated at various cross-sections in the mixing channel using equations 3.18 and 3.19. The mixing index over the range of Reynolds numbers has been depicted in Figure 4.4.

4.1.2 STM with non-Newtonian fluid (blood) as the working fluid

Numerical analysis of STM has been done with blood as a working fluid for a range of flow rates 0.00004-0.1 kg/hr. Mixing index and pressure drop have been evaluated in the given range of values of mass flow rate. It was observed that for a low mass flow rate, the flow seemed to be parallel and straight in the mixing channel. Figure 4.2 (a) can be referred for visual representation for the same. The mass transport in this region is purely governed by diffusion.

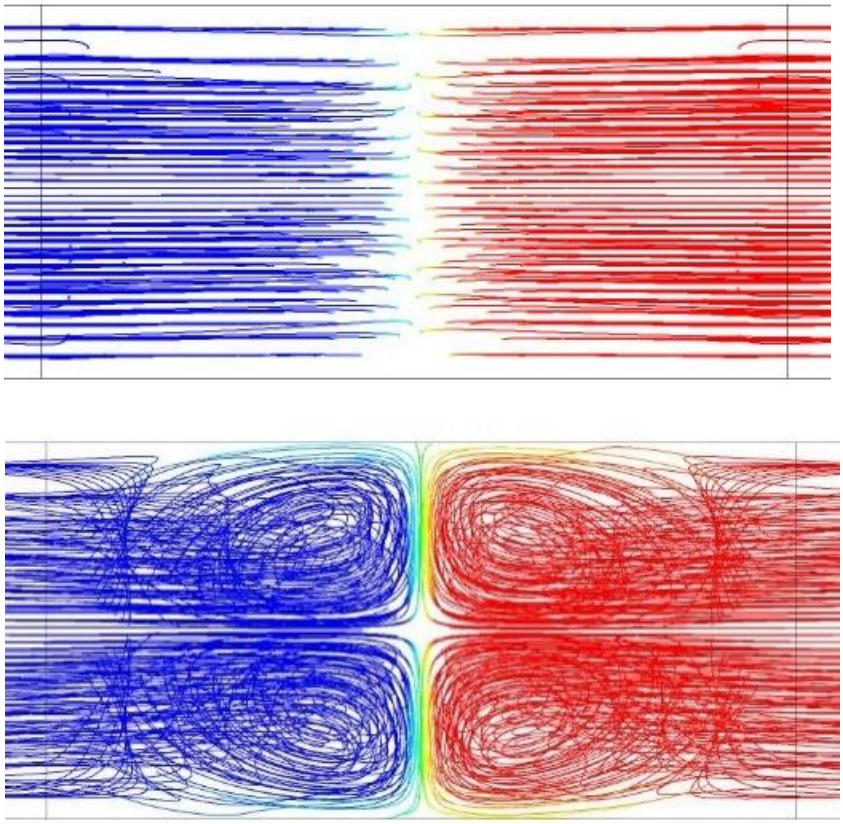

Figure 4.2 Streamlines based on species concentration inside STM for mass flow rate (kg/hr.) (a) 0.0004; (b) 0.1

The residence time is high in this region resulting in better mixing of the species. Residence time could be defined as the time spent by fluid particles inside a control volume. As the mass flow rate is increased, the residence time got decreased and hence a decrease in mixing index is observed because of the low residence time. Small vortices can be seen for mass flow rate greater than 0.04 kg/hr but, as can be seen from Figure 4.3, these small vortices do not have much impact on the mixing index because

not much improvement was observed in MI and hence the mixing of the fluid species is still governed by the mass diffusion. The mixing index experiences a decreasing-increasing trend as the Reynolds number increases. The vortex that is being created at a higher Reynolds number due to secondary flow seems to get damped by the high viscosity of the blood and hence the increase is very low. Figure 4.3 shows the graph of the variation of the mixing index Reynolds numbers.

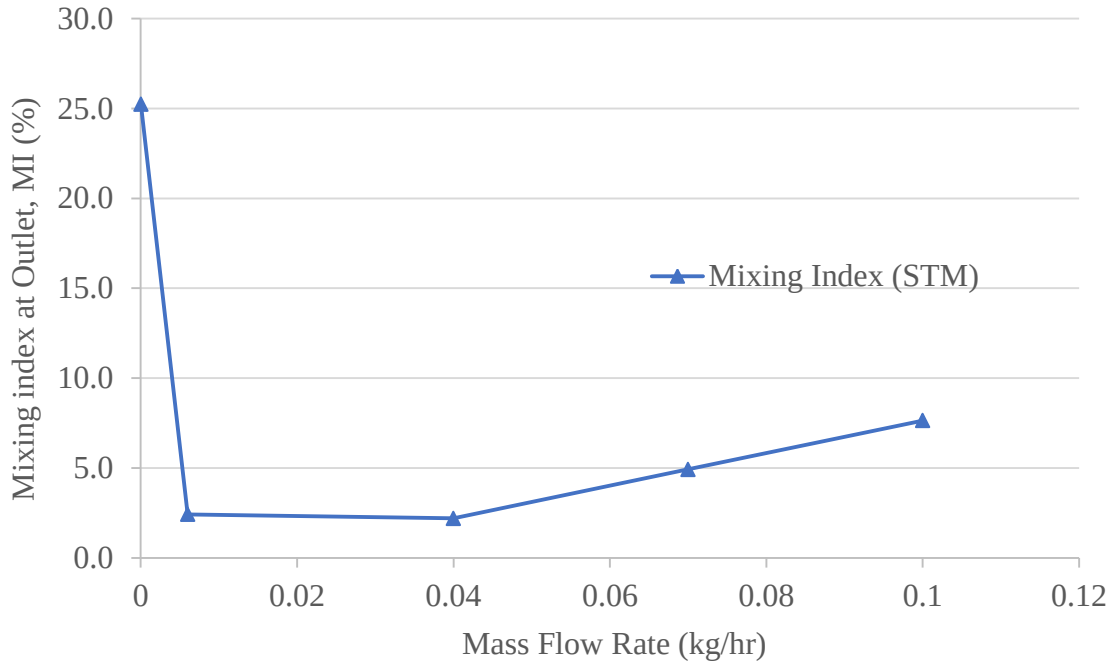

Figure 4.3 Effect of mass flow rate of blood on the mixing index at outlet for the conventional STM

4.2 Mixing and flow analysis in 3-dimensional helical micromixer with two inlets at offset (TDHM-TO)

4.2.1 TDHM-TO with Newtonian fluid (water) as the working fluid

Similarly, numerical simulation has been performed to evaluate the mixing index and pressure drop of TDHM-TO for a broad range of Reynolds numbers (8-400). Figure 4.4 presents a comparison of the mixing index of both the micromixers- STM and TDHM-TO with Reynolds numbers. Here, the mixing indexes have been calculated at the outlet of the mixing channels. As previously described in section 4.1, the mixing efficiency is very poor in STM for low Reynolds number. This is due to the flow being laminar and straight and hence results in a low mass diffusion phenomenon. As can be seen from Figure 4.4, the mixing index is further reduced to a position known as ‘critical Reynolds

number'. After this point, vortex increased with the increase in Reynolds number and this zone is called the engulfment zone.

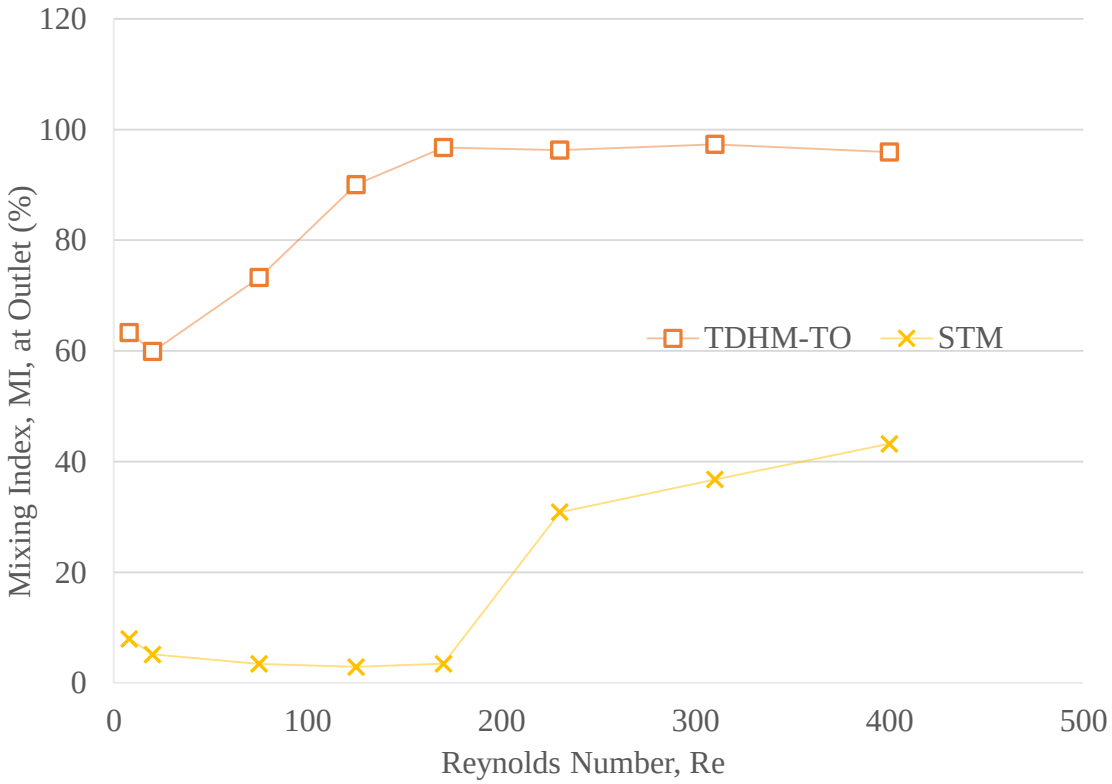

Figure 4.4 Variation of mixing index (MI) with Reynolds for STM and TDHM-TO

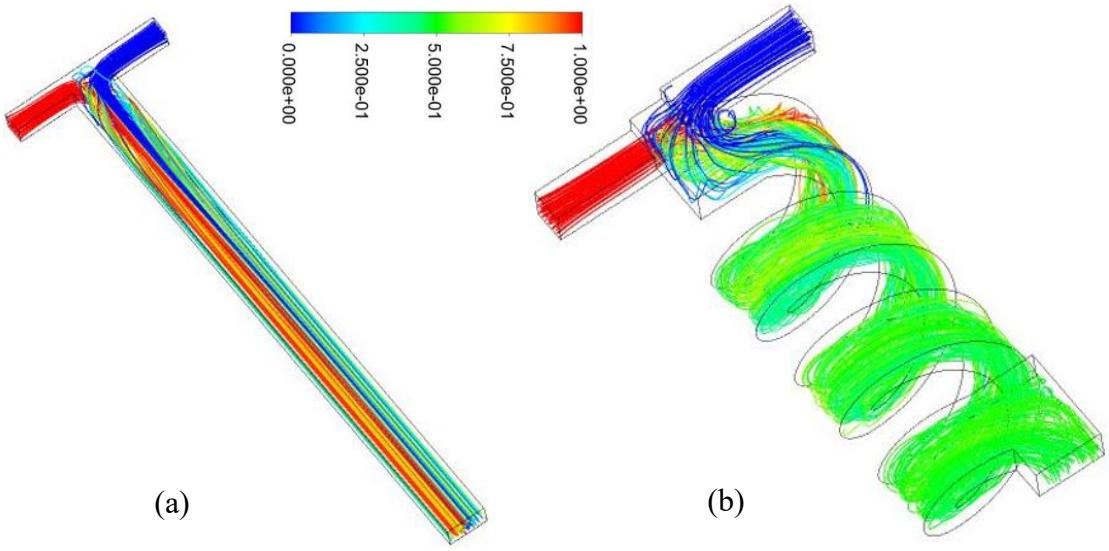

Figure 4.5 Mixing of water for (a) STM; (b) TDHM-TO at Re= 230

In this zone, the mixing of the fluid species increased due to the chaotic advection and after critical Reynolds number, the strength of secondary flow increased. As can be seen from Figure 4.4, TDHM-TO provides better mixing efficiency for all values of Reynolds numbers than STM. TDHM-TO prove to be a better option than STM. For low Reynolds number (Re ≤ 75), TDHM-TO provides more interfacial area between the fluid layers and hence stretches the fluid which increases the mass diffusion and hence the mixing index. In this range of low Reynolds number (Re≤75), the highest mixing index was found to be 73.28% for Re= 75. This value is larger than STM by 69.83%. For a higher Reynolds number (Re= 170), the mixing index was found to be 96.76% which is higher than STM by 93.27%. This is because TDHM-TO provides vortex at the inlet due to its design and also because secondary flow is dominating now that has generated due to the generation of centrifugal forces because of the three-dimensional curvature of TDHM-TO. Secondary flow usually develops around curved three dimensional surfaces. Secondary flows are perpendicular to the main direction of fluid flow. This introduces chaotic advection which increased the mixing index. Figure 4.5 shows the streamlines for STM and TDHM-TO at Re= 230 which shows the above-mentioned phenomenon.

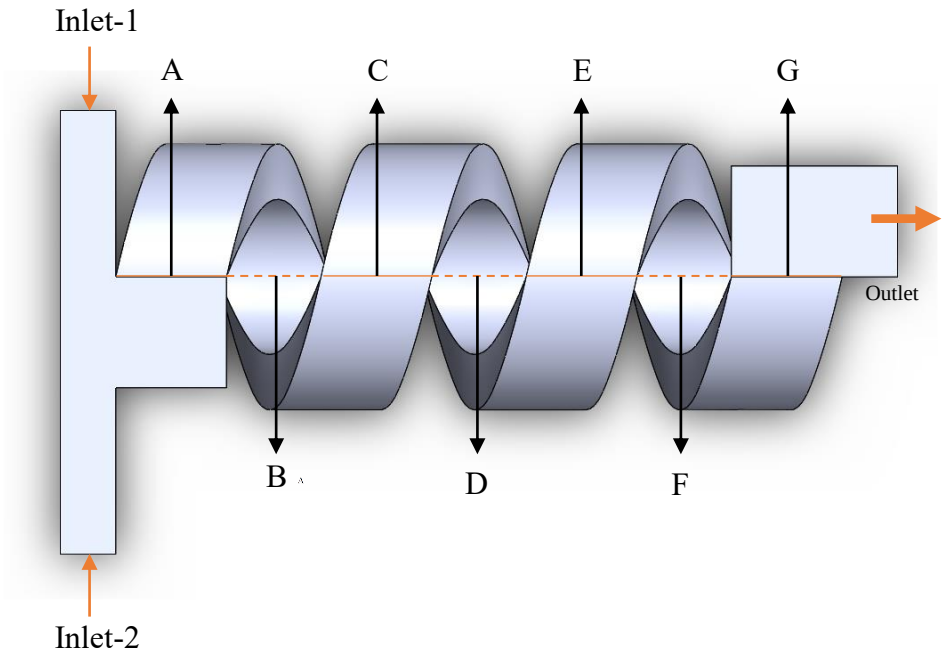

Figure 4.6 Location of planes at various section (Top View)

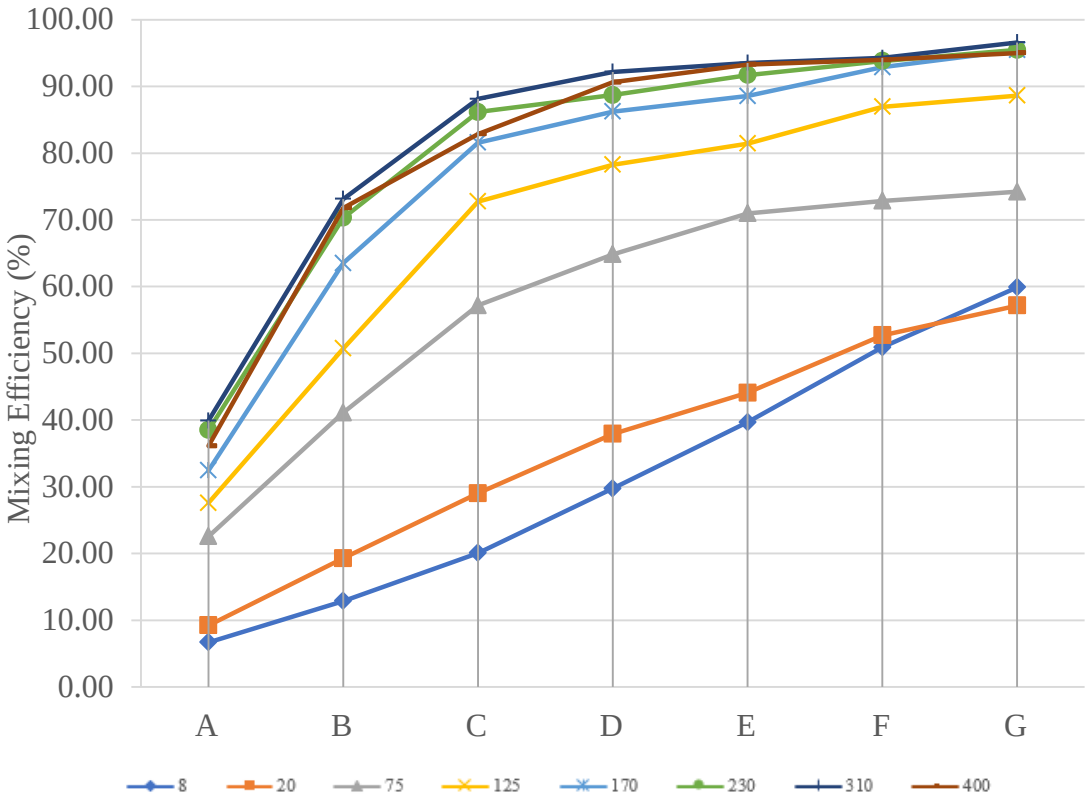

Figure 4.7 Variation of Mixing index at seven different locations in TDHM-TO

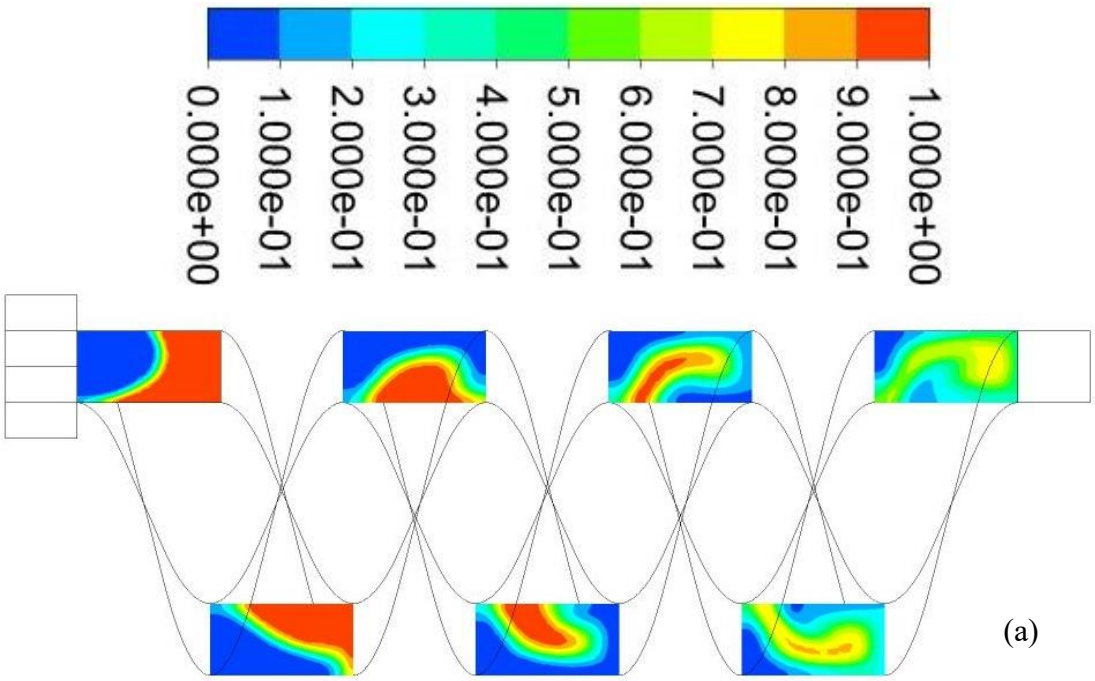

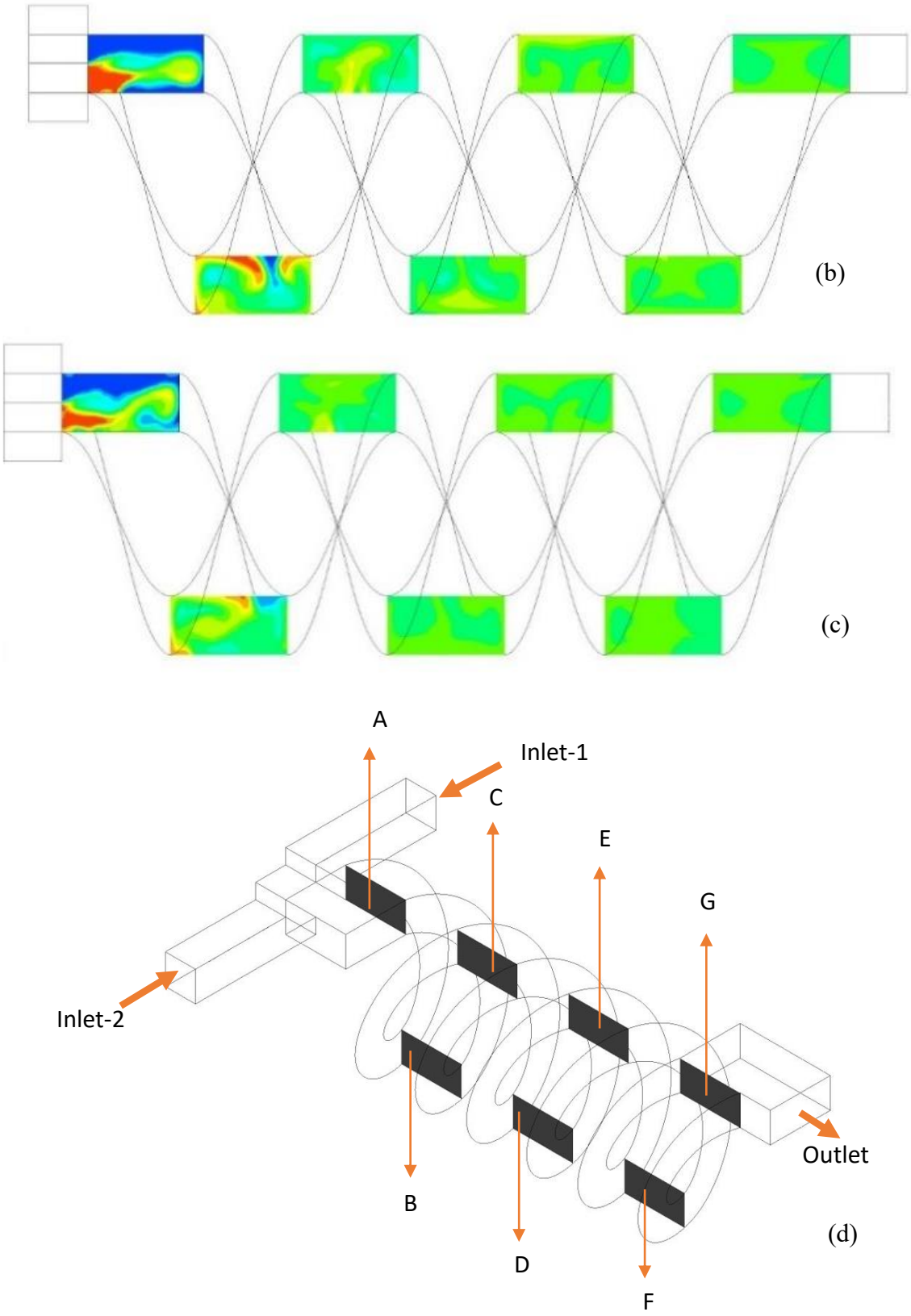

Figure 4.8 Species concentration at different sections A, B, C, D, E, F & G in TDHM-TO for Re = (a) 8; (b) 170; (c) 310; (d) Location of planes at various sections (isometric view)

An in-depth study is being done to calculate the mixing index at various locations inside the micromixer. These planes have been taken along the mixing channel length at specified distances which can be seen in the Figure 4.6 and Figure 4.8(d) which show the location of all seven planes. Figure 4.8 shows the mixing index of TDHM-TO at those planes for different values of Reynolds number. For Re= 8 and 20, the curve of the mixing index seems to be linear which, however, becomes non-linear as the Reynolds number increases. This is due to the rapid mixing of fluids. At Re= 230, the mixing efficiency increased from 38.49% at first plane A to 91.69% at plane E which is a sharp increase. This shows that a short length TDHM-TO can also be used for some specific problems. Figure 4.7 represents species concentration at various planes A, B, C, D, E, F, & G for Re= 8, 170 & 310. The mixing area appears to be small, linear and slim on initial plane A and plane B, but when the flow goes through the mixing channel, this interface between the fluid surface grows and mixing increases. This is due to the inertia of fluids which generates rotation in the fluid leading to the stretching and vortex is formed which enhances the mixing of the fluids.

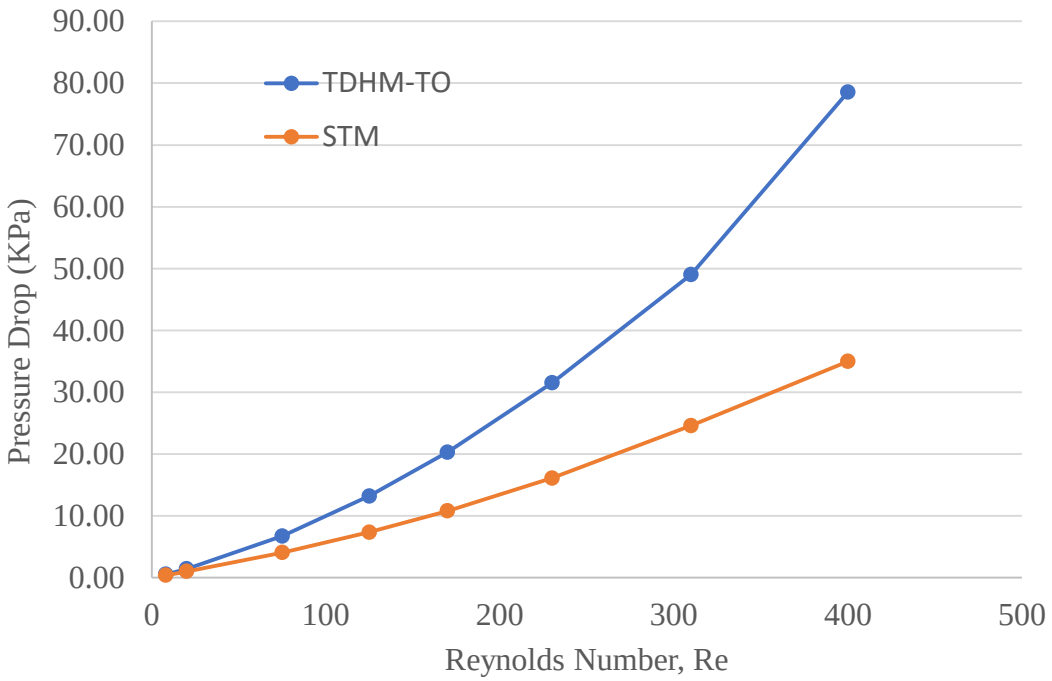

Figure 4.9 Pressure drop variation in STM and TDHM-TO with Reynolds number.

Pressure drop is a necessary parameter to calculate. This is because enhanced mixing needs increased pumping power to drive the flow of fluid species inside microchannels. Pressure drop provides the idea of required input energy and especially in passive micromixers. Figure 4.9 represents a comparison of pressure drop between STM and TDHM-TO micromixers with increasing Reynolds number. As can be seen from the Figure, no noticeable difference was found. for the low Reynolds number below, i.e., for Re= 8, but after that TDHM-TO micromixer deviated from that of STM. For all considered Reynolds numbers, TDHM-TO showed the highest pressure drop between the two.

4.2.2 TDHM-TO with non-Newtonian fluid (blood) as the working fluid

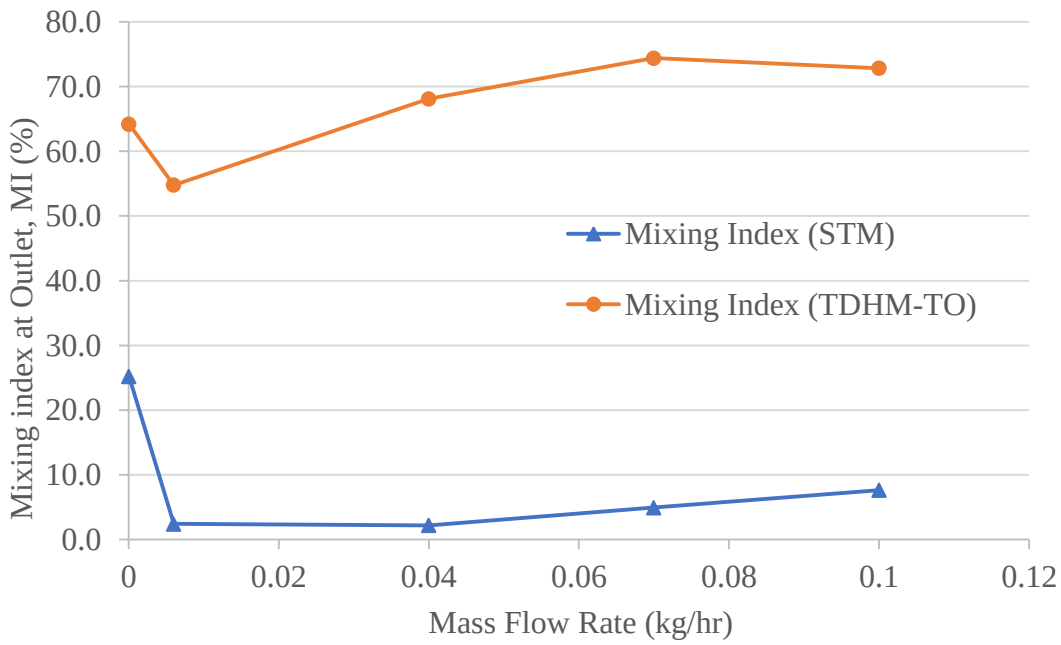

Figure 4.10 Comparison of STM and TDHM-TO based on mixing index

Figure 4.10 compares STM and TDHM-TO for mixing index and mass flow rate. As explained in the previous section 4.1, the advection time was high at a low Reynolds number and hence the mixing index is high for STM. The mixing was completely achieved by the mass diffusion of the molecules. The same goes for TDHM-TO: at a lower Reynolds number, the mixing efficiency was good due to the high residence time. However, as can be seen from Figure 4.10, TDHM-TO performed better than STM for

all values of mass flow rate. This is due to the comparatively larger interfacial area that TDHM-TO provides which helps in stretching and folding the fluid layers. The other important reason for higher mixing efficiency is the offset inlets of TDHM-TO which creates a vortex at the inlet itself. For mass flow rate 0.07 kg/hr., the mixing efficiency of TDHM-TO was observed to be 74.41% which is greater than STM by 69.48%. This is a significant increase in the mixing efficiency. Low mixing efficiency was observed for the relatively higher values of Reynolds number. This is due to the low residence time caused by the high Reynolds number which caused a drop in the mass diffusion rate. Figure 4.11 (a), (b) & (c) show the species concentration-based streamlines inside Simple T-micromixer and TDHM-TO. As can be seen from the figure, STM experiences a decreasing-increasing trend in the mixing index as seen from Figure 4.10 and the same can be observed visually from Figure 4.11(a), (b) & (c) where the flowing species can be observed to be separating from each other.

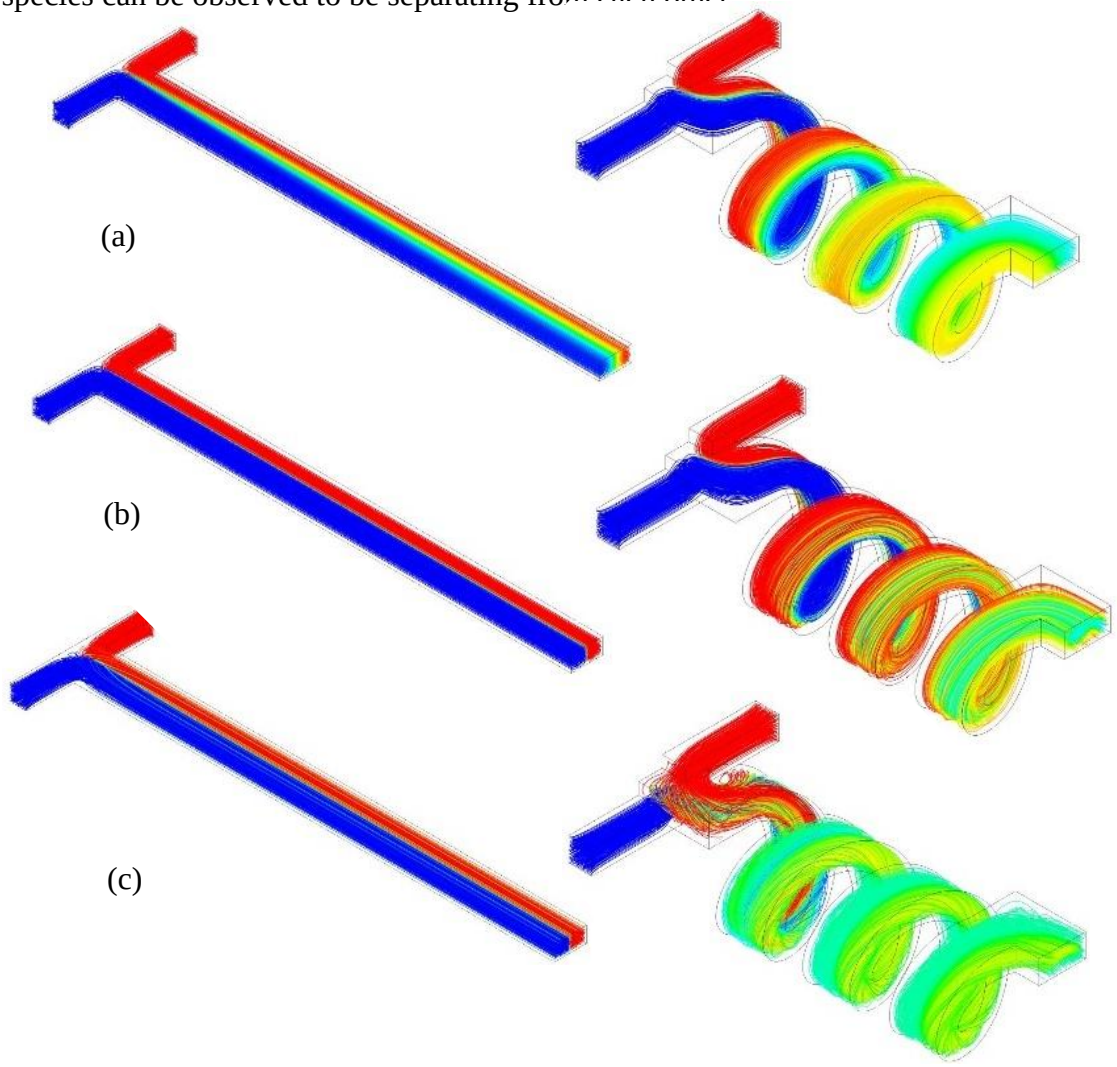

Figure 4.11 Species concentration-based streamlines inside STM and TDHM-TO for mass flow rate (a) 0.00004; (b) 0.006; (c) 0.1

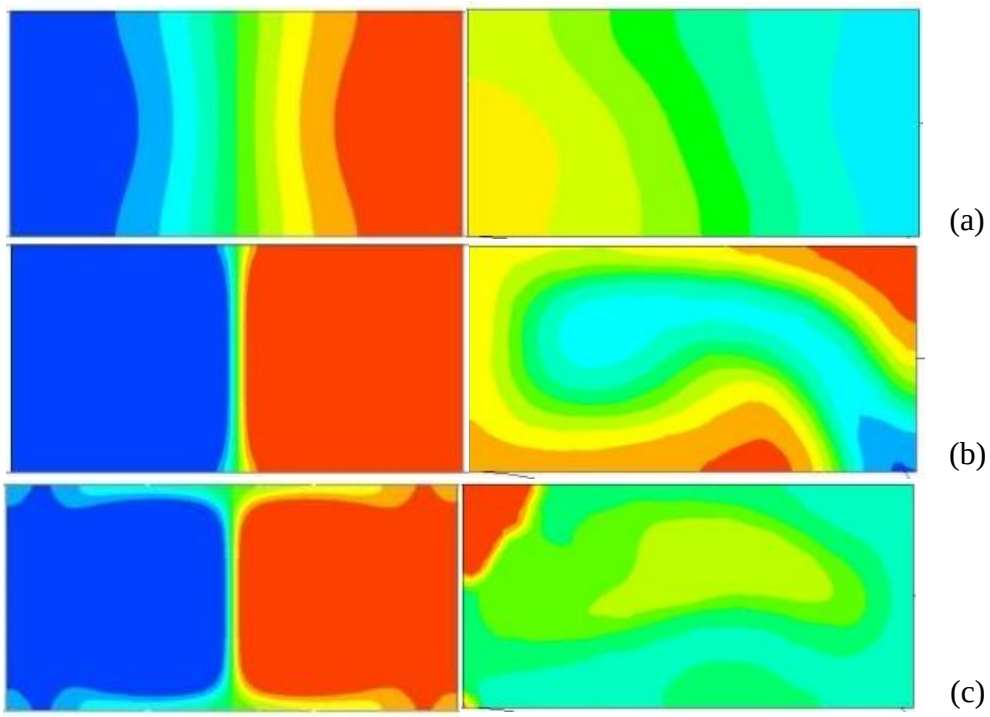

Figure 4.12 Species concentration-based contour at outlet of STM and TDHM-TO for mass flow rate (a) 0.00004; (b) 0.006; (c) 0.1

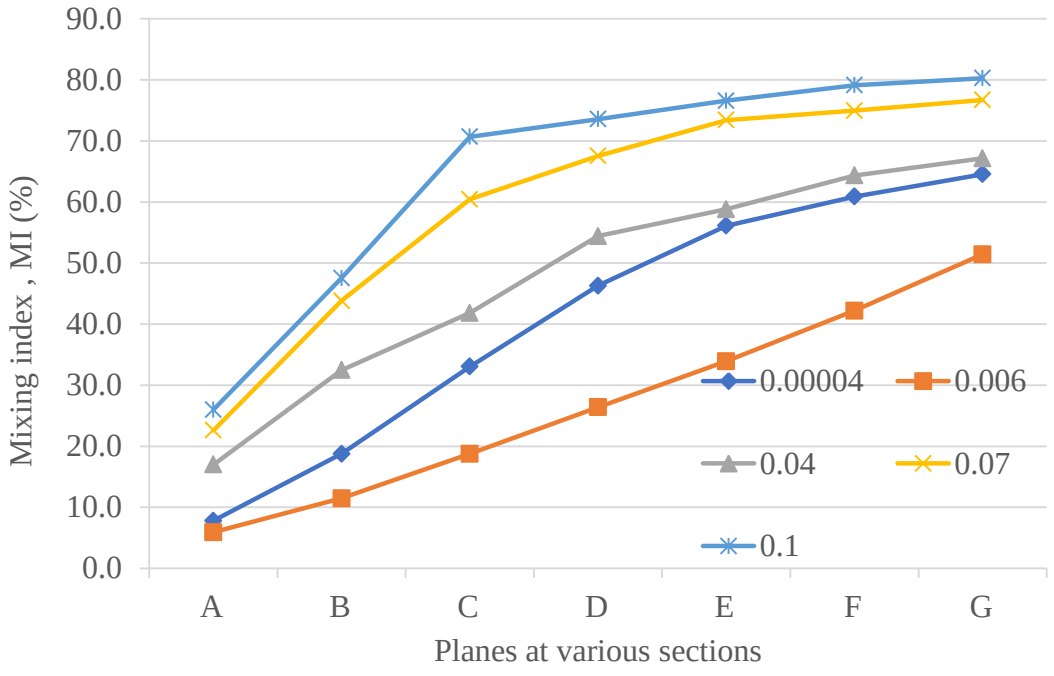

Figure 4.13 Mixing Index at seven different planes inside TDHM-TO

TDHM-TO is experiencing a decreasing-increasing pattern where it first decreases to the lowest point and then increases due to the introduction of chaotic advection introduced because of the three-dimensional shape of the micromixer. Figure 4.12 (a),

(b) shows the contour of species concentration at the outlet of STM and TDHM-TO and the above phenomenon can be observed from these illustrations also.

Seven different planes were selected inside the microchannel of TDHM-TO which were used to plot (Figure 4.6) the species concentration to get a broad understanding of the process of mixing. The figure was plotted for a high range of mass flow rate as can be seen from Figure 4.13. It can be visualized that the mixing index increases sharply from plane A to plane D for all the values of mass flow rate. For mass flow rate= 0.1 kg/hr., this increase from plane A to plane D is 47.58% which is the highest increase for any mass flow rate value. This result shows that an even smaller length microchannel can be used in some specific cases. Overall, TDHM-TO is much better compared to STM. Figure 4.14 (a), (b) show the contour of species concentration on the seven selected planes inside the microchannel.

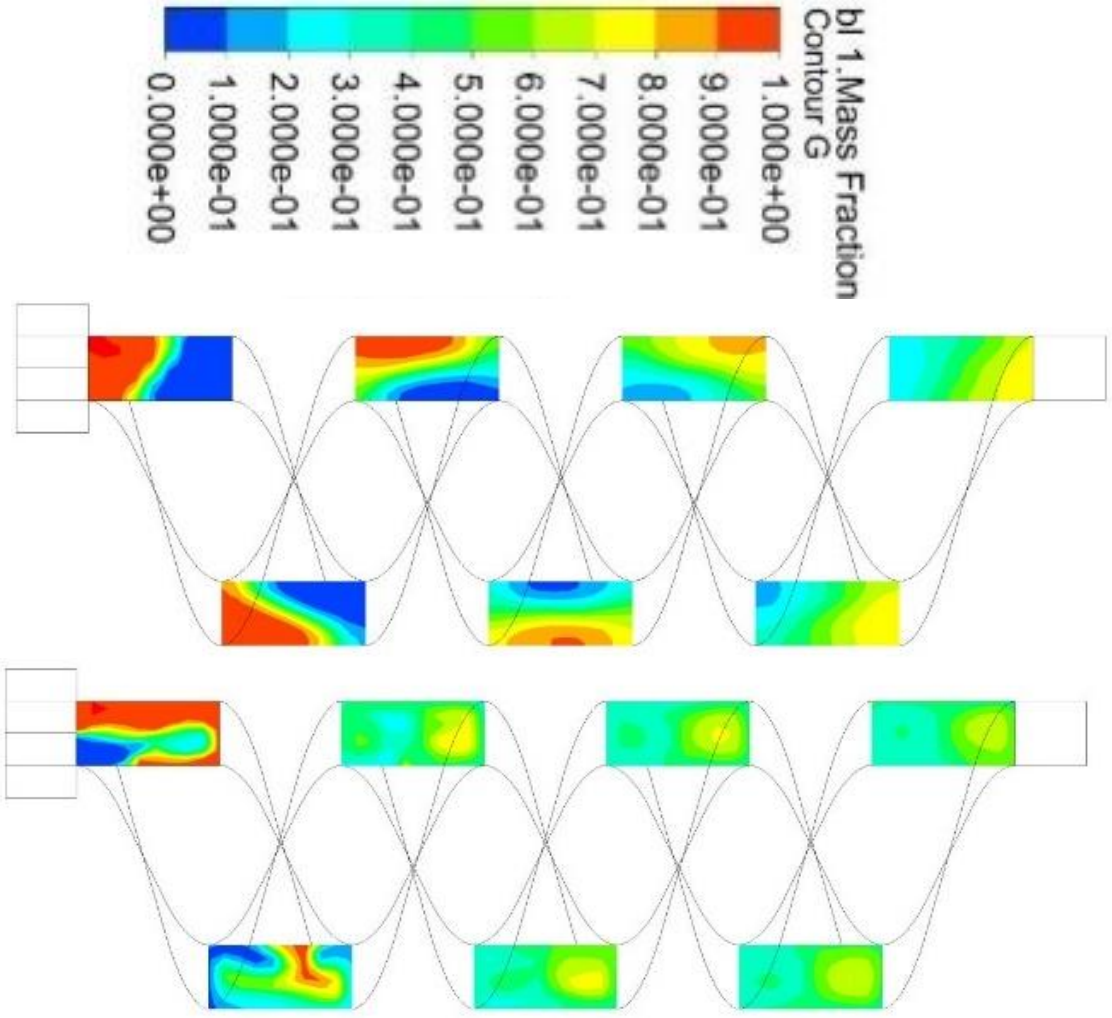

Figure 4.24 Contour of species concentration at different planes A to G inside TDHM-TO for mass flow rate = (a) 0.0004; (b) 0.1

When it comes to microsystems one of the most important parameters is power consumption. Power consumption in micromixer systems is directly related to the pressure drop and hence pressure drop becomes an important parameter to analyse. The increased mixing required more pumping power to drive the same amount of fluid. Micromotors are used to pump the fluids. Pressure drop provides an idea of the trend of power consumption, whether it will increase or decrease. Pressure drops inside Simple T- micromixer and TDHM-TO have been shown in Figure 4.15. It was observed that no noticeable difference was seen for low mass flow rate whereas the difference in pressure drop increases in both the micromixer as the flow rate increases. It can be observed from Figure 4.15 that TDHM-TO showed a relatively higher pressure drop for the values of mass flow rate.

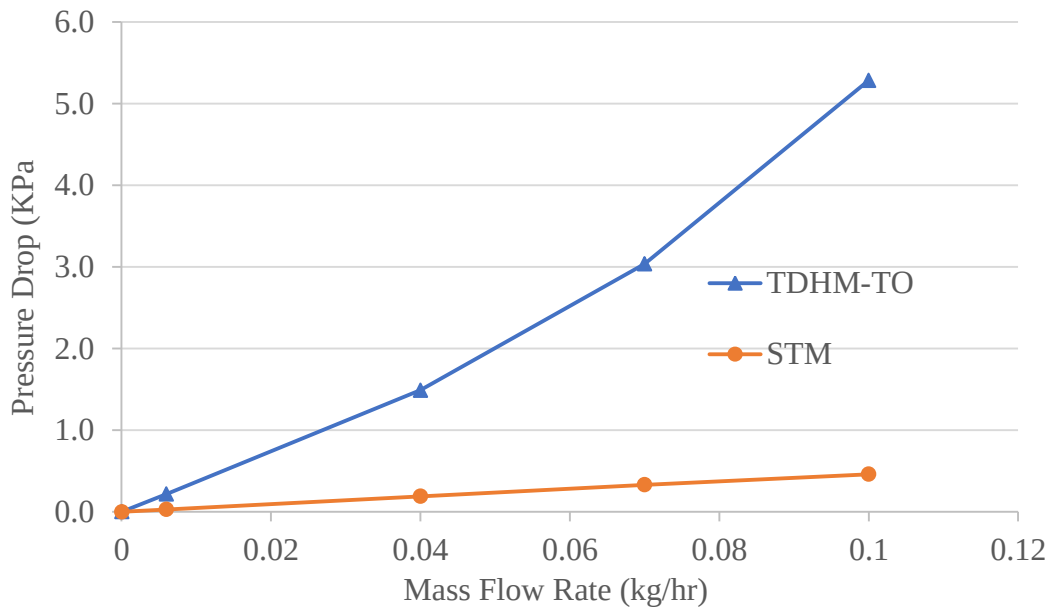

Figure 4.15 Comparison of pressure drop between STM and TDHM-TO for a range of mass flow rate

CHAPTER 5

THESIS CONCLUSION

In this paper mixing efficiency of two micromixers named Simple T-micromixer (STM), and TDHM-TO which has both inlets at offset are being studied for Newtonian fluid water and non-Newtonian fluid blood. A CFD simulation tool, ANSYS 20.1, has been used to perform the simulations. Following are the conclusions that can be made based on the simulated results. TDHM-TO provided better efficiency for all values Reynolds number and mass flow rates when compared with STM. This is due to the presence of a large interfacial area and the vortex of flow that is being created at the junction of two inlets which are placed at an offset to each other. For water, a Significant improvement of 93.27% was observed at Re= 170. This is also due to the presence of chaotic advection in the case of a high Reynolds number (Re≥125). For higher Reynolds number (Re= 400), the value of the mixing index got increased from 36.12% at plane A to 90.63% at plane D which happened in a comparatively smaller length. For blood, 69.48% of significant improvement was observed for mass flow rate= 0.07 kg/hr. An increase of 47.58% from plane A to plane D was observed for mass flow rate= 0.1 kg/hr. Hence, it can be concluded that a small length micromixer can also be used for certain applications in this particular range of Reynolds numbers. These three-dimensionally curved micromixers require less mixing length (1411.71μm) when compared with STM (3000 μm) and still produces higher efficiency. Such highly efficient devices are very useful when high accuracy is needed such as in development of vaccines and antibodies, in chemical engineering field to study chemical reactions. They use less reagents, are time-efficient, cheap and easily portable. Although the pressure drop is comparatively higher in the case of TDHM- TO when compared with STM.

5.1 Scope of future work

Future work can involve investigating the effect of various geometrical parameters like the cross-sectional area, pitch length, mean diameter of the helical curve, etc on the

mixing index and finally optimizing the micromixer from the collected data to obtain the best mixing performance in the helical channels.

Furthermore, some periodic obstructions can be introduced in the path of the flowing fluids to create disturbances which will further enhance the chaotic advection and analysis can be performed to find the optimum option for maximum mixing with a minimum pressure drop.

REFERENCES

[1] D. Nouri, A. Zabihi-Hesari, M. Passandideh-Fard, "Rapid mixing in micromixers using magnetic field", Sensors and Actuators A: Physical, 255, pp. 79-86,2017

[2] R. Article, P. Eribol, and A. K. Uguz, "Experimental investigation of electrohydrodynamic instabilities in micro channels," vol. m, pp. 425–434, 2015, doi: 10.1140/epjst/e2015-02371-5.

[3] C. A. Cortes-quiroz, A. Azarbadegan, I. D. Johnston, and M. C. Tracey, "Analysis and design optimization of an integrated micropump-micromixer operated for bio-MEMS applications," vol. 1, no. September, pp. 7–10, 2014.

[4] K. Khoshmanesh, A. Almansouri, H. Albloushi, P. Yi, and R. Soffe, "A multi-functional bubble-based microfluidic system," 2015, doi: 10.1038/srep09942.

[5] S. Qian and H. H. Bau, "Magneto-hydrodynamic stirrer for stationary and moving fluids," vol. 106, no. July 2004, pp. 859–870, 2005, doi: 10.1016/j.snb.2004.07.011.

[6] N. Veldurthi, S. Chandel, T. Bhave, and D. Bodas, "Sensors and Actuators B : Chemical Computational fluid dynamic analysis of poly (dimethyl siloxane) magnetic actuator based micromixer," *Sensors Actuators B. Chem.*, vol. 212, pp. 419–424, 2015, doi: 10.1016/j.snb.2015.02.048.

[7] B. S. Haeberle, T. Brenner, H. Schlosser, R. Zengerle, and J. Ducrøe, "Centrifugal Micromixer," no. 5, pp. 613–616, 2005, doi: 10.1002/ceat.200407138.

[8] Raza W, Hossain S, Kim K-Y, "A Review of Passive Micromixers with a Comparative Analysis", *Micromachines*, vol. 11(5), pp. 455, 2020.

[9] Okuducu MB, Aral MM, "Performance Analysis and Numerical Evaluation of Mixing in 3-D T-Shape Passive Micromixers", *Micromachines*, vol. 9(5), pp. 210, 2018.

[10] A. Mariotti, C. Galletti, M. V. Salvetti, E. Brunazzi, "Unsteady Flow Regimes in a T-Shaped Micromixer: Mixing and Characteristic Frequencies", *Ind. Eng. Chem. Res*, vol. 58, pp. 13340–13356, 2019.

[11] C. P. Fonte, D. F. Fletcher, P. Guichardon, J. Aubin, "Simulation of micromixing in a T-mixer under laminar flow conditions", *Chemical Engineering Science*, vol. 222, pp. 1-10, 2020.

[12] X. Luo, Y. Cheng, W. Zhang, Ke Li, P. Wang, W. Zhao, "Mixing performance analysis of the novel passive micromixer designed by applying fuzzy grey relational analysis", *International Journal of Heat and Mass Transfer*, vol. 178, pp. 1-14, 2021.

[13] M. Zunaid, S. Tokas, "Computational Analysis of Passive Mixing in T-Micromixer with Non-Newtonian Blood", vol. 10(3), pp. 9889–9898, 2020.

[14] R. Prakash, M. Zunaid, Samsher. "Simulation analysis of mixing quality in T-junction micromixer with bend mixing channel", *Materials Today: Proceedings*, vol. 47(13), pp. 3833-3838, 2021.

[15] J. Kurnia, A. P. Sasmito, "Performance Evaluation of Liquid Mixing in T-Junction Passive Micromixer with Twisted Tape Insert", *Industrial & Engineering Chemistry Research*, vol. 59(9), pp. 3904-3915, 2019.

[16] T. M. Dundi, V. R. K. Raju, and V. P. Chandramohan, "Numerical evaluation of swirl effect on liquid mixing in a passive T-micromixer", *Aust. J. Mech. Eng.*, 00(00), pp. 1–15, 2019.

[17] X. Chen, J. Shen, "Numerical and experimental investigation on splitting-and-recombination micromixer with E-shape mixing units", *Microsyst Technol*, vol. 23, pp. 4671–4677, 2017.

[18] X. Chen, T. Li, H. Zeng, Z. Hu, B. Fu, "Numerical and experimental investigation on micromixers with serpentine microchannels", *International Journal of Heat and Mass Transfer*, vol. 98, pp. 131-140, 2016.

[19] Mahmud, Md. Readul, "Numerical Investigation of Liquid–Liquid Mixing in Modified T Mixer with 3D Obstacles", *Journal of Engineering Advancements*, vol. 2(02), pp. 87-94, 2021.

[20] C. Y. Wu, B. H. Lai, "Numerical Study of T-Shaped Micromixers with Vortex-Inducing Obstacles in the Inlet Channels", *Micromachines*, vol. 11(12),1122, 2020.

[21] T. Li, X. Chen, "Numerical investigation of 3D novel chaotic micromixers with obstacles", *International Journal of Heat and Mass Transfer*, vol. 115, pp. 278-282, 2017.

[22] X. Shi, L. Wang, S. Huang, F. Li, "A novel passive micromixer with array of Koch fractal obstacles in microchannel", *Journal of Dispersion Science and Technology*, vol. 42(2), pp. 236-247, 2021.

[23] Z. Wu, X. Chen, "A novel design for 3D passive micromixer based on Cantor fractal structure", *Microsyst Technol*, vol. 25, pp. 225–236, 2019.

[24] B. Mondal, S. Pati, P. K. Patowari, "Fabrication of wavy micromixer using soft lithography technique", *Materials Today: Proceedings*, vol. 26(2), pp. 1271-1278, 2020.

[25] D. Tachibana, K. Matsubara, R. Matsuda, T. Furukawa, S. Maruo, Y. Tanaka, O. Fuchiwaki, H. Ota, "3D Helical Micromixer Fabricated by Micro Lost-Wax Casting", *Advanced Materials Technology*, vol. 5(1), 2020.

[26] C. Chung, YJ Chen, PC Chen, CY Chen, "Fabrication of PDMS passive micromixer by lost-wax casting", *Int. J. Precis, Eng. Manuf*, 16, pp. 2033–2039, 2015.

[27] RA Taheri, V. Goodarzi, A. Allahverdi, "Mixing Performance of a Cost-effective Split-and-Recombine 3D Micromixer Fabricated by Xurographic Method", *Micromachines*, vol. 10(11), 786, 2021.

[28] M. Kumar, J. Rajiyan, P. Gupta, "A computational approach for solving elasto-statics problems", *Materials Today: Proceedings*, vol. 46(15), pp. 6876-6879, 2021.

[29] P.R. Mashaei, S. Asiaei, S.M. Hosseinalipour, "Mixing efficiency enhancement by a modified curved micromixer: A numerical study," *Chemical Engineering and Processing - Process Intensification*, vol. 15, 2020, doi: 10.1016/j.cep.2020.108006.

[30] A. Afzal and K. Y. Kim, "Mixing performance of passive micromixer with sinusoidal channel walls," *J. Chem. Eng. Japan*, vol. 46, no. 3, pp. 230–238, 2013, doi: 10.1252/jcej.12we144.

[31] Xin Wang, Zhanqiang Liu, Yukui Cai, Bing Wang, Xichun Luo, "A cost-effective serpentine micromixer utilizing ellipse curve," *Analytica Chimica Acta*, vol. 1155 2021, 10.1016/j.aca.2021.338355.

[32] L. Balasubramaniam, R. Arayanarakool, S. D. Marshall, B. Li, P. S. Lee, and P. C. Y. Chen, "Impact of cross-sectional geometry on mixing performance of spiral microfluidic channels characterized by swirling strength of Dean-vortices," *J.*

Micromechanics Microengineering, vol. 27, no. 9, 2017, doi: 10.1088/1361-6439/aa7fc8.

[33] M. Rafeie, M. Welleweerd, A. Hassanzadeh-Barforoushi, M. Asadnia, W. Olthuis, and M. E. Warkiani, "An easily fabricated three-dimensional threaded lemniscate-shaped micromixer for a wide range of flow rates," *Biomicrofluidics*, vol. 11, no. 1, 2017, doi: 10.1063/1.4974904.

[34] J. Yang, L. Qi, Y. Chen, and H. Ma, "Design and fabrication of a three dimensional spiral micromixer," *Chinese J. Chem.*, vol. 31, no. 2, pp. 209–214, 2013, doi: 10.1002/cjoc.201200922.

[35] K. Liu *et al.*, "A high-efficiency three-dimensional helical micromixer in fused silica," *Microsyst. Technol.*, vol. 19, no. 7, pp. 1033–1040, 2013, doi: 10.1007/s00542-012-1695-6.

[36] C. Shan, F. Chen, Q. Yang, Z. Jiang, and X. Hou, "3D multi-microchannel helical mixer fabricated by femtosecond laser inside fused silica," *Micromachines*, vol. 9, no. 1, pp. 1–7, 2018, doi: 10.3390/mi9010029.

[37] A. Husain, N. Z. Al-Rawahi, F. A. Khan, and A. Samad, "Blood flow and mixing analysis in split-and-recombine micromixer with offset fluid inlets," *Am. Soc. Mech. Eng. Fluids Eng. Div. FEDSM*, vol. 3, pp. 1–5, 2018, doi: 10.1115/FEDSM2018-83468.

[38] J. Boyd, J. M. Buick, and S. Green, "Analysis of the Casson and Carreau-Yasuda non-Newtonian blood models in steady and oscillatory flows using the lattice Boltzmann method," *Phys. Fluids*, vol. 19, no. 9, 2007, doi: 10.1063/1.2772250.

[39] A. Afzal and K. Y. Kim, *Flow and mixing analysis of non-Newtonian fluids in straight and serpentine microchannels*, vol. 116. Elsevier, 2014.

[40] F. Abraham, M. Behr, and M. Heinkenschloss, "Shape optimization in steady blood flow: A numerical study of non-Newtonian effects," *Comput. Methods Biomech. Biomed. Engin.*, vol. 8, no. 2, pp. 127–137, 2005, doi: 10.1080/10255840500180799.